- Dynamics, predictability, impacts, and climate change considerations of the catastrophic Mediterranean Storm Daniel (2023)
- 3 Emmanouil Flaounas<sup>1,2</sup>, Stavros Dafis<sup>3</sup>, Silvio Davolio<sup>4,5</sup>, Davide Faranda<sup>6, 7, 8</sup>, Christian Ferrarin<sup>9</sup>,
- 4 Katharina Hartmuth<sup>1</sup>, Assaf Hochman<sup>10</sup>, Aristeidis Koutroulis<sup>11</sup>, Samira Khodayar<sup>12</sup>, Mario Marcello
- 5 Miglietta<sup>13</sup>, Florian Pantillon<sup>14</sup>, Platon Patlakas<sup>2,15</sup>, Michael Sprenger<sup>1</sup>, Iris Thurnherr<sup>1</sup>

- 8 1. Institute for Atmospheric and Climate Science, ETH Zurich, Zurich, Switzerland
- 9 2. Institute of Oceanography, Hellenic Centre for Marine Research, Athens, Greece
- 10 3. National Observatory of Athens, Institute for Environmental Research and Sustainable
- 11 Development, I. Metaxa & Vas. Pavlou, P. Penteli (Lofos Koufou), 15236 Athens, Greece
- 12 4. Dipartimento di Scienze della Terra, Università di Milano, Milan, Italy
- 13 5. Institute of Atmospheric Sciences and Climate, National Research Council, Bologna, Italy
- 14 6. Laboratoire des Sciences du Climat et de l'Environnement, UMR 8212 CEA-CNRS-UVSQ,
- 15 Université Paris-Saclay & IPSL, CE Saclay l'Orme des Merisiers, 91191 Gif-sur-Yvette, France
- 16 7. London Mathematical Laboratory, 8 Margravine Gardens, London W6 8RH, UK
- 17 8. LMD/IPSL, ENS, Université PSL, École Polytechnique, Institut Polytechnique de Paris, Sorbonne
- 18 Université, CNRS, Paris France
- 19 9. CNR National Research Council of Italy, ISMAR Institute of Marine Sciences, Venice, Italy
- 20 10. Fredy and Nadine Herrmann Institute of Earth Sciences, Hebrew University of Jerusalem,
- 21 Edmond Safra Campus, Jerusalem, Israel
- 22 11. School of Chemical and Environmental Engineering, Technical University of Crete, 73100
- 23 Chania, Greece
- 24 12. Mediterranean Centre for Environmental Studies (CEAM), Charles R. Darwin Street, 14 46980
- 25 Paterna, Valencia (Spain)
- 26 13. Institute of Atmospheric Sciences and Climate, National Research Council, Padua, Italy
- 27 14. Laboratoire d'Aérologie, Université de Toulouse, CNRS, UPS, IRD, Toulouse, France
- 28 15. Department of Physics, National and Kapodistrian University of Athens, Athens, Greece

29 30

Correspondence to: Emmanouil Flaounas (emmanouil.flaounas@env.ethz.ch)

31

# 33 Abstract

- 34 In September 2023, Storm Daniel formed in the central Mediterranean Sea, causing significant
- 35 socioeconomic impacts in Greece, including fatalities and severe damage to agricultural
- 36 infrastructure. Within a few days, it evolved into a tropical-like storm (medicane) that made landfall
- 37 in Libya, likely becoming, to our knowledge, the most catastrophic and lethal weather event ever
- 38 documented in the region.
- 39 This study places Storm Daniel as a centerpiece of the disasters in Greece and Libya. We conducted a
- 40 comprehensive analysis that links a cyclone system with hazardous weather conditions relevant to
- 41 extreme precipitation, floods, and significant sea wave activity. In addition, we examine Daniel's
- predictability in different development stages and draw connections with previous case studies. Given the climatologically extreme precipitation produced by Daniel, we examine the capacity of numerical
- 44 weather prediction models to capture such extremes and we finally investigate potential links to
- 45 climate change.
- 46 Daniel initially developed like any other intense Mediterranean cyclone, including medicanes, due to
- 47 upper tropospheric forcing followed by Rossby wave breaking. At this stage, it produced significant
- 48 socioeconomic impacts in Greece. As it intensified and attained tropical-like characteristics, it
- 49 developed markedly just prior to landfall, reaching peak intensity over land. Considering short lead
- 50 times (around four days), cyclone formation exhibited low predictability, whilst landfall in Libya was
- more predictable.. Our analysis of impacts highlights that numerical weather prediction models can
- 52 capture the extreme character of precipitation and flooding in both Greece and Libya, providing
- 53 crucial information on the expected severity of imminent flood events.

We also examine moisture sources contributing to extreme precipitation. Our findings indicate that large-scale atmospheric circulation was the primary driver, drawing substantial water vapor from the eastern Mediterranean, Black Sea and continental Europe. The intensification of storm Daniel was likely driven by anomalously warm SST in the Mediterranean and Black Sea, enhancing evaporation and contributing to the extreme precipitation along the Lybian coast. Finally, our analysis supports interpreting its impacts as characteristic of human-driven climate change but also highlights the exceptionality of this cyclone, especially in its medicane phase, which complicates the comparison with other cyclones.

#### 1. Introduction

In early September 2023, a low-pressure system developed within the central Mediterranean Sea, close to Greece. Due to the expected severity of the event, on 4 September 2023, the Hellenic National Meteorological Service named the upcoming Storm 'Daniel'. Daniel evolved into a deep cyclone within a few days and began moving erratically southward. On the 8th, it shifted eastward and eventually made landfall along the coast of Libya as a powerful system (Fig. 1a). Daniel led to substantial, unprecedented socio-economic impacts in the Central-Eastern Mediterranean from 4 to 11 September 2023.

In the cyclogenesis stage, on 5 September 2023, the weather station network of the National Observatory of Athens in Greece (NOAAN; Lagouvardos et al., 2017) measured more than 750 mm of accumulated daily rainfall in the eastern part of the Thessaly region (flooded areas are shown in cyan colours in Fig. 1b) and up to 1235 mm within four days. Thessaly experienced flooding that led to 17 fatalities, the loss of 25% of Greece's annual agricultural production, and the destruction of the local road network. About five days later, on 10 September 2023, the cyclone made landfall near Benghazi, Libya. As a result, northeastern Libya's population of 884,000 people has been affected directly in five governorates by the collapse of two dams. About 30% of the city of Derna was flooded (Fig. 1c), and almost 900 buildings, roads, and other infrastructures were destroyed in the area (OCHA 2023, UNICEF 2023). According to the DTM update (IOM 2023), over 5,000 people were presumed dead, 3,922 deaths were registered in hospitals, 10,000 people were declared missing by the Libyan government and Red Crescent Society, while at least 30,000 people were recognized as internally displaced (UNICEF 2023, IOM 2023) in the Derna area. Extensive damage affected critical infrastructure such as hospitals and drinking water supply systems. Many roads were rendered impassable, making humanitarian aid and supplies difficult. At least a \$10 million budget was allocated from the UN Central Emergency Response Fund to scale up intervention in response to the Libya disaster, and almost \$72 million were requested to cope with the most urgent needs of around 250,000 people (OCHA 2023) just for the first three months after the flooding.

Daniel was an intense cyclone, preceded by Rossby wave breaking over the Atlantic Ocean, which led to the formation of an omega blocking pattern (Couto et al., 2024) and the subsequent intrusion of an upper-level trough in the Mediterranean. This scenario is commonly observed before the formation of intense Mediterranean cyclones, including medicanes (Raveh-Rubin and Flaounas, 2017). From the perspective of atmospheric dynamics, upper tropospheric systems are often precursors of Mediterranean cyclogenesis. Such systems force ascent by advancing upper level PV structures. (Flaounas et al., 2022). While the formation of Mediterranean cyclones is almost entirely dependent on baroclinic instability, the development and intensification of a cyclone into a deep low-pressure system is also a function of diabatic processes. More precisely, latent heat release close to the cyclone centre, mainly due to convection, is a source of positive PV anomalies at low levels, eventually translating into enhanced cyclonic circulation. Therefore, baroclinic instability and latent heat release are the main forcings. Both processes drive cyclones' intensification from the cyclogenesis stage until maturity, i.e., when the cyclone reaches its minimum pressure at the centre. A complete review of Mediterranean cyclone dynamics is available by Flaounas et al. (2022), while a recent thorough analysis of the interplay and synergies between baroclinic and diabatic forcing of another intense cyclone in the central-eastern Mediterranean (Ianos, 2020) is provided by Pantillon et al. (2024).

108

109

111

112

113

115

116

117

118

119

As an environmental hazard, cyclones may produce heavy precipitation from the stage of genesis until their lysis, close to their centres but also in remote areas due to localized convective cells (Raveh-Rubin and Wernli, 2016), warm conveyor belts and frontal structures (Pfahl et al., 2012; Flaounas et 110 al., 2018). Regardless of whether precipitation is stratiform or convective, the large-scale atmospheric circulation contributes by transporting water vapour toward the Mediterranean and thus "feeding" the cyclone-induced precipitation (Flaounas et al., 2019; Hochman et al., 2024). Indeed, the Mediterranean basin is composed of a relatively closed sea surrounded by continental areas. 114 Consequently, Mediterranean cyclones have fewer water sources than their counterparts over the open oceans. In these regards, large-scale ventilation of water vapour from the Atlantic Ocean and other remote regions towards the Mediterranean has been shown in numerous cases to enhance heavy precipitation, together with local evaporation due to cyclone-induced high wind speeds (Duffourg and Ducrocq, 2011; Flaounas et al., 2019; Khodayar et al., 2021; Sioni et al., 2023). Hence, identifying and quantifying the contribution of water sources to heavy precipitation is a key step for improving 120 our ability to forecast socio-economic impacts in the Mediterranean (Hochman et al., 2022a; Khodayar et al., 2025).

125

126

127

128

129

130

131

132

133

From a climatological standpoint, cyclones are responsible for most of the wind and precipitation extremes within the Mediterranean (Nissen et al., 2010; Flaounas et al., 2015; Hochman et al., 2022b). Therefore, cyclones play a central role in the compoundness of high-impact weather events (Catto and Dowdy, 2021; Rousseau-Rizzi et al., 2023; Portal et al., 2024), also considering that relatively compact systems close to the coast additionally contribute to impacts with storm surges and significantly high waves (Patlakas et al., 2021; Ferrarin et al., 2023a; Ferrarin et al., 2023b). Especially in the case of precipitation, recent results have shown that intense water vapour transport and Rossby-wave breaking are the two main features that lead to extreme Mediterranean events (de Vries, 2021; Hochman et al., 2023). Both of these large-scale atmospheric features favour the development of cyclones into deep, low-pressure systems: the first through baroclinic forcing and the latter through diabatic forcing by intensifying convection (e.g., Davolio et al., 2020). Thus, their understanding is crucial for predicting socio-economic impacts on weather and climate scales.

134 135 136

137

138 139

140

141

142

143

144

145

Future trends in cyclone-induced hazards in the Mediterranean are mainly quantified through downscaling experiments (e.g., Reale et al., 2022) or statistical-deterministic methods that generate synthetic tracks (e.g., Romero and Emanuel, 2017; Sandler et al., 2024). Nevertheless, additional investigation is needed to assess the role of climate change in the intensification of storms that occur in the current climate. While attributing extreme events, such as medicanes and high-impact extratropical storms, is a rather tricky task, recent studies based on analogues have suggested that several recent storms are more intense than would have been expected in the absence of climate change (Faranda et al., 2022, 2023). Further investigation of this critical topic requires a case-by-case approach to take into account the particularities of each storm and to acquire a more holistic understanding of the specific processes related to cyclone intensity that are also affected by climate change.

146 147 148

149

150

151

152

153

154

155

156

When a high-impact weather event occurs, it encompasses multiple interconnected aspects often studied separately. First, understanding the event's dynamics and physical processes is crucial for assessing and interpreting weather forecasting performance and climate change attribution. Second, the associated hazards—such as floods and windstorms—must be assessed according to the specific weather conditions, as well as the vulnerability and exposure of the affected areas. Despite their interdependence, all these aspects of a specific weather event are rarely examined through an integrated approach. Our motivation is thus to apply a comprehensive framework to provide an interdisciplinary assessment of the Storm Daniel event. In particular, we aim to address the following four questions:

- 157 How did cyclone development stages relate to flooding in Greece and Libya? 1.
- 158 2. How reliable and accurate were numerical models for predicting weather conditions and river 159 discharges at different lead times?
- 160 3. Can numerical weather prediction models adequately simulate climate extremes?
- 161 4. Can we link Storm Daniel's characteristics to climate change?

The following section describes the datasets and methods, while Section 3 briefly describes the storm dynamics. Section 4 analyses Storm Daniel's predictability, and Section 5 discusses the potential contribution of natural variability and human-induced climate change to the characteristics and evolution of Storm Daniel..

## 2. Datasets and methods

## 2.1 Datasets

To analyze the evolution of the cyclone and assess its predictability, we use the operational analysis and the ensemble prediction system (EPS) products of the European Centre for Medium-Range Weather Forecasts (ECMWF). Since the last model upgrade at ECMWF (Cycle 48r1), operational analysis and medium-range ensemble forecast data have been available at a grid spacing of about 9 km. The increase in horizontal resolution and improvements in the data-assimilation system led in substantial improvements in forecast skill (ECMWF Newsletter, 176, 2023). The EPS comprises 50 members that are initialized with a perturbed analysis using slightly modified model physics, along with a control forecast. This probabilistic forecasting system has been designed to provide a range of possible weather conditions up to 15 days in advance, offering an estimation of predictability. Finally, to assess Daniel's climatological aspects, we used ERA5 reanalysis (Hersbach et al., 2020) which provides hourly atmospheric fields at a 0.25-degree grid spacing.

We used river discharge data from the Global Flood Awareness System (GloFAS; Grimaldi et al., 2022) to investigate the hydrological impacts of Daniel across Greece and Libya. GloFAS, an integral component of the Copernicus Emergency Management Service (CEMS), provides global operational flood forecasts. It integrates the open-source LISFLOOD hydrological model with ERA5 meteorological reanalysis data, interpolated to match the GloFAS resolution (0.05° for version 4.0), and is produced at a daily frequency. This dataset includes historical discharge records essential for establishing discharge climatology from 1993 to 2023. To assess flood forecast potential, we also employed data from the European Flood Awareness System (EFAS). EFAS utilises the open-source LISFLOOD hydrological model, calibrated at a higher spatial resolution of approximately 1.5 km over European latitudes. Forecasts are issued twice daily, initialized at 00 and 12 UTC, and provide lead times ranging from 5 to 15 days to capture a wide range of potential weather conditions affecting river discharge. These forecasts incorporate data from the 51 members of the ECMWF EPS, the Deutsches Wetter Dienst (DWD) high-resolution forecasts, and the 20-member COSMO Local Ensemble Prediction System (COSMO-LEPS), ensuring a comprehensive analysis of forecast capability. For this study, we usedEFASforecasts driven by the 51 ECMWF EPS ensemble members.

Finally, to evaluate Daniel's marine and coastal impacts, we analyzed wave data from the Mediterranean Sea Waves Analysis and Forecast system (Korres et al., 2023), available through the Copernicus Marine Service (CMEMS). Additionally, wave climatology was derived using the Mediterranean Sea wave reanalysis dataset (1993-2021; Korres et al., 2021), also provided by CMEMS.

#### 2.2 Methods

## 2.2.1 Object diagnostics

We identify two-dimensional objects of extreme precipitation to assess the predictability of major impacts in the EPS forecasts. These objects are defined separately for each member of the EPS as neighbouring grid points where daily precipitation values exceed the 99th percentile in the ERA5 climatology (1990-2020). Using these objects, we define the probability of the EPS forecasts predicting extreme weather associated with Daniel. Similarly, we define the likelihood of cyclone occurrence in the EPS by identifying cyclone masks in each ensemble member, based on the outermost mean sea level pressure (MSLP) contour enclosing an area smaller than that of a circular

216 disc with a 200 km radius.

#### 2.2.2 Air parcel trajectories and moisture source diagnostic

Ten-day air parcel backward trajectories were calculated at 20 hPa intervals between 1000 and 300 hPa from starting locations on a regular latitude-longitude grid with a 30 km, within defined boxes over Greece and Libya (as shown in Fig. 1a), using the LAGRANTO tool (Wernli and Davies, 1997; Sprenger and Wernli, 2015). We computed two sets of backward trajectories: (i) the first concerns Storm Daniel, with trajectories initialized every 6 hours on 5 September 2023 and 11 September 2023 from the Greece and Libya boxes, respectively, using six-hourly 3D wind fields from the ECMWF operational analysis data; (ii) the second concerns air parcel trajectories based on ERA5 reanalysis wind fields and corresponds to the 100 most extreme daily precipitation events in each region. These trajectories were initialized from the same grid points in the Greece and Libya boxes as in the first set. The 100 extreme events were identified as the days with the highest number of grid points within the Libya or Greece regions recording daily surface precipitation exceeding the 90th percentile for autumn (1990 - 2023). Storm Daniel is included among the 100 most extreme daily precipitation events in both regions. Along all trajectories, we interpolated specific humidity, relative humidity, and the boundary layer height pressure.

We identified moisture sources in Daniel and the 100 most extreme daily precipitation events using the moisture source diagnostic developed by Sodemann et al. (2008). This method tracks changes in specific humidity along all trajectories that precipitate upon arrival, which are defined as air parcels showing a decrease in specific humidity during the last time step before arrival and a relative humidity larger than 90% upon arrival (following Sodemann et al., 2008). Along each trajectory, an increase in specific humidity is interpreted as a moisture uptake, while a decrease indicates moisture loss. Each moisture loss reduces the contribution of preceding moisture uptakes, weighted by the magnitude of each uptake.

For a detailed description of the moisture source diagnostic, see Sodemann et al. (2008). In our analysis, moisture uptakes along each trajectory were weighted by the decrease in specific humidity during the last step before arrival. Relative moisture uptakes were then computed across all trajectories for each six-hourly time step, gridded onto a global 1° latitude-longitude grid, and averaged daily. These values are expressed in 10<sup>-5</sup> % km<sup>-2</sup>, indicating each grid cell's relative contribution per km<sup>2</sup> to precipitation in the target region. Finally, the daily relative moisture sources averaged over the 100 most extreme events wereused as a climatological reference for Daniel.

# 2.2.3 The role of natural variability and human-driven climate change

We applied the methodology developed in the framework "ClimaMeter" (see Faranda et al. 2024, for more details). ClimaMeter offers a dynamic approach to contextualizing and analyzing weather extremes within a climate context. This framework provides both an accessible, immediate contextualization of extreme weather events and a more in-depth technical analysis after their occurrence.

In this study, we investigate how Mediterranean depressions affecting Greece and Libya have changed in the present climate (2001–2022; factual period) compared to how they would have appeared in the past climate (1979–2000; counterfactual period). To this end, we compute analogues of MSLP anomalies associated with Storm Daniel using data from the MSWX database (Beck et al., 2022). We then identify significant differences between the present and past analogues in terms of MSLP, near-surface temperature, precipitation, and wind speed.

To account for the seasonal cycle in MSLP and temperature, we remove the average pressure and temperature, we remove the climatological daily mean values for each calendar day at every grid point. Total precipitation and wind-speed data are not preprocessed. If the duration of the event is longer than one day, we apply a moving average across the duration of the event for all variables. We examined all daily MSLP within each period and select the best 15 analogues, i.e., those that minimize the Euclidean distance to the event, representing roughly the smallest 1% Euclidean distances in each subset. We tested extracting between 10 to 20 analogues and found no qualitatively

significant variations in the results. As is standard in attribution studies, the event itself is excluded from the present period analysis.

Following Faranda et al. (2022), we define several diagnostic quantities to support the interpretation of analogue-based attributions. These quantities are then compared between the counterfactual and factual periods. The quantities are:

- Analogue Quality (Q): Q is the average Euclidean distance of a given day from its 29 closest analogues. If the value of Q for the extreme event belongs to the same distribution as its analogues, then the event is not unprecedented, and attribution can be performed. If the Q value exceeds its analogues, the event is unprecedented and not attributable.

- Predictability Index (D): Using dynamical systems theory, we can compute the local dimension D of each SLP map (Faranda et al., 2017). The local dimension is a proxy for the number of active degrees of freedom of the field, meaning that the higher the D, the less predictable the temporal evolution of the MSLP maps will be (Faranda et al., 2017). If the dimension D of the event analyzed is higher or lower than its analogues, then the extreme will be less or more predictable than the closest dynamical situations identified in the data.

- Persistence Index ( $\Theta$ ): Another quantity derived from dynamical systems theory is the persistence  $\Theta$  of a given configuration (Faranda et al., 2017). Persistence estimates the number of days we will likely observe a situation analogous to the one under consideration.

Finally, to account for the possible influence of low-frequency modes of natural variability in explaining the differences between the two periods, we also considered the potential roles of the El Niño-Southern Oscillation (ENSO), the Atlantic Multidecadal Oscillation (AMO), and the Pacific Decadal Oscillation (PDO). We performed this analysis using monthly indices produced by NOAA/ERSSTv5. Data for ENSO and AMO were retrieved from the Royal Netherlands Meteorological Institute (KNMI) Climate Explorer. At the same time, the PDO time series was downloaded from the NOAA National Centers for Environmental Information (NCEI). The significance of the changes between the distributions of variables during the past and present periods was evaluated using a two-tailed Cramér-von Mises test at the 0.05 significance level. If the p-value is smaller than 0.05, the null hypothesis that both samples are from the same distribution is rejected, namely, we interpret the distributions as being significantly different. We use this test to determine the role of natural variability.

### 3. Atmospheric processes leading to impacts

### 3.1 Cyclogenesis stage and impacts in Greece

Before Daniel formed, an omega-blocking pattern and an anticyclonic Rossby wave-breaking occurred over Europe (Couto et al., 2024). Wave breaking resulted in the intrusion of an upper-level PV streamer into the central Mediterranean basin, triggering cyclogenesis in the Ionian Sea on 4 September 2023, which eventually led to the formation of Daniel within 24 hours (marked by the northernmost, first track point in Fig. 1a). Figure 2a shows that the cyclone on 5 September 2023 was located between Italy and Greece, developing as a moderate low-pressure system with a minimum MSLP value of about 1004 hPa. The PV streamer in the upper troposphere wrapped cyclonically around the cyclone centre (green contour in Fig. 2a), indicating an ongoing baroclinicity which contributed to the cyclone's development. Accordingly, a high wind speed pattern follows the PV streamer's orientation with larger values over the Balkans and at the northwest side of the cyclone (wind barbs in Fig. 2a). This configuration summarises a typical dynamical structure of Mediterranean cyclones at a stage preceding maturity, i.e., the time of maximum intensity (Flaounas et al., 2015).

Accumulated precipitation also follows the typical structure of Mediterranean cyclones, with higher amounts on the northeast side of the cyclone centre (Flaounas et al., 2018). Figure 2a shows that at the cyclone's initial stages, the highest precipitation accumulation was observed in central Greece

328

329

330

332

333

334

335

336

337

338

339

340 341

342

343

344

345

346

347

348

349

350

351

352

353

354

355

356

357

358

359

360

361 362

363

364

365

366

367 368

369

370

371372

373

374 375

376

377

378

379 380 (Dimitriou et al., 2024). NOAAN surface stations recorded more than 750 mm of daily rainfall and up to 1,235 mm within four days in the eastern parts of the Thessaly region (flooded areas are shown in cyan colours in Fig. 1b). Notably these peak values are underestimated by about 40% in the ECMWF analysis (with a max IFS 24-h accumulated rainfall of 434 mm on 6 September 2023 00 UTC).

To quantify the contribution of local and remote areas to such an intense precipitation event in Greece, Fig. 3a identifies the areas where moisture uptake has been significant for the air parcels that reached the flooded region of Thessaly (blue square in Fig. 3a). Considering the largest moisture uptakes that contribute at least 50% to the catastrophic precipitation in Greece (dashed black contour in Fig. 3a, which primarily separates the green from the red colours), major sources were found in the Aegean and the Black Seas. This tilted southwest-to-northeast orientation of essential water sources follows the pathway of strong winds blowing over the Balkans and the eastern Mediterranean (wind barbs in Fig. 2a), having a similar orientation as the upper-level PV streamer. The intense sea surface fluxes induced by easterly winds are a precursor feature common to other cyclones developing in the same area (e.g., Miglietta et al., 2021). Further moisture mainly originated from central to eastern Europe and the North Atlantic Ocean. These source regions generally agree with a recent study (Argüeso et al., 2024), which investigated moisture sources of rainfall over Greece from 3 to 9 September 2023 using a Eulerian moisture source diagnostic. Our moisture source analysis shows larger contributions from land (54.7%) than in Argüeso et al. (2024) (27%). The Lagrangian method used in our study indicates relatively large moisture contributions from the north of the Black Sea because most of the air parcels arriving on 5 Sep 2023 descended and took up moisture in this region before moving southwestward along the western flank of the PV streamer. The differences in the land fraction between the two methods might originate from different periods used for the moisture source calculations, different handling of moisture uptakes above the boundary layer, a lower explained fraction of the total moisture sources (84%) with the Eulerian compared to the Lagrangian diagnostic (explained fraction of 90%), and general differences in Eulerian versus Lagrangian approaches. An ongoing comparison study of moisture source diagnostics investigates differences in these methods in detail and will shed more light on disagreements between various moisture source diagnostics. Overall, the moisture sources agree well with the climatology of moisture sources of the Mediterranean cyclones that produce the heaviest precipitation events (Flaounas et al., 2019). The moisture sources shown in Fig. 3a largely overlap with the climatological moisture sources of extreme precipitation in the same area. However, for Daniel, they are mainly concentrated over the Aegean Sea and regions to the northeast. In contrast, the typical moisture sources for extreme precipitation in Thessaly extend further over the central Mediterranean (Fig. 3b).

The hydrological impacts of Storm Daniel were profound and unprecedented. Figure 4 compares the peak mean daily river discharge during Daniel with historical records over three decades, integrating the cumulative hydrological impacts over the entire event. Figure 4a shows the spatial distribution of the maximum simulated peak discharge from January 1993 to August 2023 (i.e., before Daniel), demonstrating typical peak discharge patterns in the Eastern Mediterranean. In contrast, Fig. 4b compares the event-wide mean daily peak discharge during September 2023, when Daniel occurred, against the historical peak river discharges of the last 30 years (Fig. 4a). Results reveal an unprecedented magnitude of Daniel's impacts, with several areas experiencing river discharges that exceeded the historical maximums by 300 to 500%. The darkest shades in Fig. 4b indicate the most heavily affected regions, where the river discharge during Daniel exceeded previous records by at least a factor of five, highlighting that Daniel was an unprecedented event of increased river discharge levels (further discussed in section 5). At this cyclone stage, 17 human casualties were registered in Thessaly, along with a profound hydrological aftermath. The extreme rainfall from 3 to 8 September 2023 led to widespread flooding across 1,150 km<sup>2</sup> in the Thessalian plain, 70% of which was agricultural land. The inundation severely affected the cotton crops, with floodwaters covering more than 282 km<sup>2</sup>, roughly 30% of the region's total cotton fields. Over 35,000 farm animals were also affected (He et al., 2023).

## 3.2 Mature stage and impacts in Libya

Severe weather gradually faded in Greece during the night of 6 September 2023 while the surface cyclone moved southwards in phase with the upper-tropospheric low. In the following three days, Daniel lingered over the central Mediterranean Sea (circular part of the track in Fig. 1a), with minimum pressure remaining almost constant, close to 1004 hPa (Fig 1a). Figure 5a, b shows the sea surface temperature (SST) anomaly in the area affected by Storm Daniel on 3 and 9 September, respectively. Before the passage of Storm Daniel, positive SST anomalies dominated the study area, with values exceeding 1°C between the Libyan coast and Greece, and lower anomalies (0 to 0.5°C) observed east of Sicily. Following the storm's passage, a significant drop in SST resulted in an extensive area of negative anomalies greater than 1°C between Libya and Greece. A colder SST core with a decrease of less than 1.5°C was observed east of Sicily, while the northern Aegean Sea experienced an even more pronounced decline. Such SST cooling after the passage of medicanes has been previously diagnosed using explicitly resolved air-sea interactions in coupled atmosphere-ocean models (Ricchi et al., 2017; Bouin and Lebeaupin Brossier, 2020; Varlas et al., 2020) and SST observations (Avolio et al., 2024). Nevertheless, the feedback mechanism between cyclone intensity and SST cooling is expected to be less important than the one typically observed in tropical cyclones.

The role of anomalously high SSTs in intensifying cyclones has been previously shown in several studies based on numerical sensitivity experiments (Miglietta et al., 2011; Romaniello et al., 2015; Messmer et al., 2017; Pytharoulis, 2018; Argüeso et al. 2024; Sanchez et al. 2024). In the case of Daniel, deep moist convection was favoured, as suggested by the great extent of the areas covered by cold cloud-tops and intense lightning activity close to the cyclone centre (not shown). Subsequently, on 8 September, the cyclone started showing tropical-like features, like a deep warm core, spiral cloud bands, and a maximum wind speed in the low levels a few tens of km from the centre. Thus, the cyclone satisfies the phenomenological definition of a medicane recently proposed (Miglietta et al., submitted). Deep convection contributed to the rapid deepening of the cyclone, which reached a minimum MSLP of 997 hPa on 10 September 2023, 18 UTC, after making landfall at the northeastern coasts of Libya around 10 September 2023, 06 UTC (Fig. 1).

A comparison of Figs. 2a and 2b shows that, at the time of maturity, the area covered by at least 2 PVUs at 300 hPa is significantly smaller than during cyclogenesis. Nevertheless, Fig. 2b shows that the 2-PVU patch is collocated with the cyclone center, advected from the west. Hewson et al. (2024) proposed that this collocation is responsible for the cyclone's intensification just before landfall. The intensification of a Mediterranean cyclone due to the synergy of upper-level baroclinic forcing and deep convection is a common characteristic of intense Mediterranean cyclones, including medicanes (Flaounas et al., 2021). A previous case of a medicane intensifying due to the collocation of a PV streamer with the cyclone center was documented by Chaboureau et al. (2012). This phenomenon reflects, on the one hand, the anomalous nature of this medicane (since medicanes generally intensify over the sea and weaken inland), on the other hand, the critical role of upper-level features in the evolution of Mediterranean cyclones.

At the same time, Daniel developed a significantly stronger MSLP gradient, leading to wind speeds reaching up to 40 knots (about 20 m s<sup>-1</sup>). The intense winds associated with the storm generated a severely disturbed sea in the Central Mediterranean basin, with south-westward propagating waves extending from the Aegean Sea to Libya following the strong winds pathway (Fig. 2b). Indeed, the analysis of the wave data from the Mediterranean Sea Waves Analysis and Forecast shows waves with significant height of about 5 m in the Gulf of Sirte and the northern Aegean Sea (Fig. 6a). Such values exceed the 99th percentile in the Mediterranean Sea wave reanalysis. A peculiar aspect of Daniel is that strong winds blew in the Central Mediterranean Sea for many days. As a result, Daniel preserved a severe sea state over northern Greece, in the Central Mediterranean basin, and along the Libyan coast. To evaluate the cumulative impact of the event, we computed the total storm wave energy (TSWE; Arena et al., 2015) by integrating the wave power contribution of each sea state over the storm duration (Fig. 6b). TSWE reached peak values of about 3000 kWh m<sup>-1</sup> in the Gulf of Sirte, which is above the 99th percentile of the total storm wave energy obtained from the Mediterranean Sea wave reanalysis. Such an energetic sea condition and the storm surge affected much of Libya's

eastern coastal zones, causing coastal flooding, erosion, and infrastructure damage (World Bank, 2023).

436 437 438

439 440

441

442

443

444

445

446

447

448

449

450

451

452

453

454

435

In terms of precipitation, Storm Daniel also presented exceptional features, During the cyclone's mature stage, Bayda experienced about 414.1 mm of rainfall within less than 24 hours, equaling 80% of the city's mean annual accumulated precipitation and a new daily precipitation record ( World Meteorological Organisation, 2023a). It is worth mentioning that simulated 24-hr total accumulated precipitation on 11 September 2023 in Libya, up to 382 mm, was not located within the Derna catchment, as discussed in Hewson et al. (2024), the most impacted area. Significant moisture sources (red colours in Fig. 3c) encompass the cyclone centre, with more than 50% of the moisture originating from the Mediterranean Sea. This suggests that the cyclone-induced circulation played an essential role in moistening the atmosphere within the proximity of the cyclone. Nevertheless, the largest moisture sources that contribute collectively at least 50% of the total precipitation in Libya (black dashed contour encompassing green to red colours in Fig. 3c) still retain a southwest-to-northeast orientation as in Fig. 3a (i.e., during the precipitation event in Greece). Comparing the moisture sources between the two precipitation events in Greece and Libya, the cyclone tends to attract more moisture from its surrounding area in the latter case. In contrast, in both cases, northern moisture sources tend to align with the large-scale circulation responsible for downstream cyclogenesis in the Mediterranean. This southwest-northeast orientation of moisture sources contrasts with the climatological sources in Figs. 3b and 3d which mainly highlight the importance of local sources, especially from the Mediterranean Sea westwards of the two study regions.

455 456 457

458

459

460

461

462

463

464

465

466

467

468

469

470

471

472

473 474

475

476

Figure 4 highlights the region's exceptional river discharges, as in Greece's case. However, the absence of similarly strong discharge signals in several severely impacted regions, such as the wider Pelion area in Greece and Derna (Libya), is notable and can be attributed to several factors. First, the GloFAS model has limitations in spatial resolution and calibration. The model operates at a resolution of approximately 5 km (0.05°), which, while adequate for global-scale flood awareness, is insufficient for resolving localized hydrological dynamics. For instance, the catchments east of Volos, including the wider Pelion area, are approximately 30 km<sup>2</sup>, while the Derna basin spans around 575 km<sup>2</sup>. In both cases, localized rainfall-runoff dynamics are critical in shaping discharge patterns, particularly during extreme events. Due to insufficient in-situ discharge data, the absence of Greece and Libya in the GloFAS calibration dataset further exacerbates these limitations since the model relies on generalized parameter regionalization rather than site-specific calibration, introducing significant uncertainties into discharge predictions. Furthermore, inaccuracies in the rainfall inputs depicted in Figure 2 propagate into the discharge simulations shown in Figure 4. For instance, within the Peneus catchment, the maximum recorded 24-hour accumulated precipitation was 274 mm at Zappeio and 226 mm at Neraida stations, as Dimitriou et al. (2024) reported, while accumulations of up to 750 mm were recorded outside the catchment, specifically over the Pelion area, east of Volos. In the Wadi Derna catchment, extreme rainfall exceeded 400 mm day<sup>-1</sup>, with torrential rainfall ranging between 150 and 240 mm across several locations and Al-Bayda recording a maximum of 414.1 mm (World Meteorological Organisation, 2023b). These rainfall extremes were underrepresented in the GloFAS rainfall inputs, propagating into the discharge simulations and contributing to the muted signals observed in Figure 4(b).

477 478 479

480

481

482

483

484

485

486

487

488

#### 4. Weather forecasting of Daniel and implications for impacts

Daniel's impacts took place in two distinct periods: during cyclogenesis and at maturity. In the former stage, most precipitation was produced in areas far from the cyclone centre, drawing moisture from the surrounding areas. At the later stage, the cyclone impacts were relevant to landfall, and precipitation and sea level rise were significant close to the cyclone centre. Therefore, the two distinct stages of Daniel that provoked substantial impacts in Greece and Libya were linked to cyclone stages of different dynamics, which also have further implications for Daniel's numerical prediction. In the case of Greece, i.e., at the initial stage of Daniel, it is the timely prediction of cyclogenesis that would have primarily provided useful information to civil protection, whereas, in the case of Libya, it would have been the accurate prediction of the cyclone track, intensification, and its landfall location. This

 section focuses on the predictability of the environmental hazards linked to Daniel's socio-economic impacts, i.e., precipitation amounts, sea state, and cyclone track.

## 4.1 Forecasting the cyclogenesis stage

Concerning the cyclogenesis stage, a forecast model has to predict the formation of the cyclone to provide valuable information regarding its impact. This suggests that numerical weather prediction models should accurately reproduce the large-scale atmospheric circulation, the Rossby wave breaking, and the consequent intrusion of the PV streamer within the Mediterranean, as shown in Fig. 2a by the green contour. Such a large-scale circulation pattern is absent from forecasts initialised one week ahead (Fig. 7a). At a lead time of 120 hours, the PV streamer is present, though its location shows high uncertainty among EPS members(Fig. 7c). Indeed, the PV distribution of all EPS members at 300 hPa (outlined by coloured crosses in Fig. 7) depicts a much larger area of possible high PV values than the one in Fig. 2a. This is due to the limited agreement on the occurrence -or colocation- of the intrusion of the PV streamer among the EPS members, ranging between 25 to 50%, as suggested by the blue crosses in Fig. 7c.

Following the uncertainty in the PV streamer occurrence, the cyclone is also absent from the MSLP ensemble average one week ahead (black contour in Fig. 7a). The MSLP spread seems consistent within the shown domain (about 1 to 3 hPa). At subsequent lead times, higher spread of MSLP tends to concentrate close to the cyclone centre (Figs. 7c and 7e) until it becomes negligible 24 hours before cyclogenesis (Fig. 7g). At such a short lead time, the cyclone formation was forecast with confidence to occur in the Ionian Sea, to the southwest of Greece (black contours in Fig. 7g). Confident forecasts of cyclogenesis should go hand in hand with higher agreement among the EPS members on the location of the PV streamer. Indeed, 24 hours before cyclogenesis, more than 95% of EPS members agreed on the area of PV streamer intrusion. Accordingly, average values (blue contour in Fig. 7g) better match the ones in the ECMWF analysis (green contour in Fig. 2a).

To get deeper insights into the representation of cyclogenesis among the EPS members, Fig. 8 shows the level of agreement on the cyclone objects (as presented in section 2.2.1). At a lead time of 168 hours, cyclogenesis forecast was relatively poor (Fig. 8a). Still, at a lead time of 120 hours (Fig. 8c), cyclone centres are present (red dots in Fig. 8), scattered in the central Mediterranean but still close to the actual location where the cyclone initially formed. Higher overlapping of cyclone objects among the EPS members (green shading in Fig. 8) is indeed within the limits of the observed cyclone object, as in the ECMWF analysis (black contour in Fig. 8c). In fact, about 30% of the different EPS members produce overlapping cyclone objects. At a forecast lead time of three days, the overlapping of cyclone objects increases clearly (comparing green shaded areas between Figs 8c and 8e), suggesting higher agreement among the EPS members on the cyclone occurrence within the correct location. The high agreement is retained even for shorter lead times (Fig. 8g).

The similar behaviour in the cyclone and PV streamer predictability relies on the direct relationship between the Rossby wave breaking over the Atlantic Ocean and the accurate prediction of Mediterranean cyclogenesis. This has been highlighted by Chaboureau et al. (2012) and Pantillon et al. (2013) for the case of the extratropical transition of a hurricane upstream of a medicane, more recently by Portmann et al. (2020) for another case, and has been demonstrated by Sherrmann et al. (2023) in a semi-idealized framework. In the case of Daniel, Hewson et al. (2024) similarly suggested the role of the extratropical transition of Hurricane Franklin as responsible for the high uncertainty one week ahead. Only in forecasts initialized after the extratropical transition has occurred is the PV streamer predicted to intrude on the Mediterranean, thus explaining the contrast between 5 and 7 days lead times. A similar "jump" in the predictability of cyclone occurrence has been shown for several medicane cases by Di Muzio et al. (2019). Most probably, this "jump" is due to the dependence of Mediterranean cyclogenesis on the preceding Rossby wave breaking and, consequently, on the credible inclusion of this event within the forecast initial conditions.

## 4.2 Forecasting cyclone location and intensity at the mature stage

Figure 1a shows that on 10 September, Daniel made landfall on the coasts of Libya. For all different forecast lead times of this event, the spread of MSLP consistently retains high values close to the landfalling area (right column of panels in Fig. 7). This is directly relevant to the high MSLP gradients close to the cyclone centre (Fig. 2b) where even "small" displacement of cyclone centres may result in a relatively large standard deviation of MSLP in the EPS. Indeed, Figs. 8b and 8d point to the high certainty of the cyclone occurrence in the EPS, where most members produce consistent and overlapping cyclone objects (depicted by dark green shading). Such performance comes in contrast to forecasting the stage of cyclogenesis, where MSLP spread does not have a clear pattern (the left panels of Fig. 7, green and yellow areas), and cyclone objects present limited overlapping for the same lead times (e.g., comparing Figs. 8c and 8d). The limited agreement among the EPS members on the PV streamer intrusion leads to considerable differences among the EPS members on the location or even the occurrence of cyclogenesis. In contrast, the predictability of landfall in Libya seems more consistent among the EPS members of ECMWF.

Considering a forecast lead time of 120 hours (i.e., initialization on 6 September), the cyclone has already formed and was located over the central Mediterranean (just before the spiral part of the track). Therefore, the cyclone has already been inscribed in the model's initial conditions. Still, from the perspective of impacts, the location of landfall and the cyclone's intensity are crucial. Figure 9a shows that even for an early lead time of five days (initial conditions of 5 September 2023, 0000 UTC), the cyclone tracks from all EPS members make landfall on the Libyan coasts. The spread of the tracks is wide enough to include the actual cyclone track (in blue colour in Fig. 9a); therefore, the forecast may lead to a reliable and timely warning of potential impacts.

Nevertheless, Fig. 9b shows that almost all the EPS members underestimated the cyclone's intensity by forecasting too high MSLP values on 10 September at the time of landfall. The intensity of the cyclone is dependent on the baroclinic and diabatic forcing of its development (Flaounas et al., 2021). Therefore, the performance of all EPS members depends on the accurate representation of the parametrized processes, mainly convection close to the cyclone centre and surface fluxes, and the morphology of the PV streamer intrusion. For the present case, Hewson et al. (2024) noted that, while in the development stage the latent heat released from convection, favoured by the high SST and intense sea surface fluxes, balanced out the tendency for frictional decay, in the last stage a marked upper-level low moving from the west (marked by high PV values in Fig. 7h) was responsible for a further deepening. Upper tropospheric forcing is crucial in accurately predicting cyclone intensity in this context. While Fig. 7b —unlike Fig. 7a— shows that some EPS members align with the location of this upper tropospheric feature (blue crosses), an average of 2 PVU and an agreement above 50% among the EPS members near the cyclone center is only evident at a lead time of approximately three days (Fig. 7f, depicted by green crosses).

### 5. Daniel's impacts in a climatological context

## **5.1 Forecasting climate extremes**

The previous sections focused on the capacity of the EPS to forecast Daniel's cyclogenesis as the primary driver of impacts. In this section, we extend this analysis by focusing on the predictability of hazards in a climatological context, namely extreme precipitation and consequent floods. We used the ERA5 reanalysis to diagnose extremes since this product offers a reliable and consistent representation of present-day climate (Hersbach et al., 2020). In this respect, the left column of Fig. 10 shows the area affected by extreme daily precipitation on 5 September (in red contour, explained in Section 2.2.1). In addition, Fig. 10 shows the percentage of the EPS members that forecast daily precipitation exceeding the climatological threshold for extremes, defined by the 99th percentile of daily precipitation in ERA5 (in blue shading). At a lead time of 120 hours (Fig. 10c), less than half of the ensemble members predicted the climatological extreme precipitation amounts within the area delimited by the climatological values of ERA5 (red contours). Nevertheless, the area formed by the blue shading in Fig. 10c is consistent with the climatological extremes. The members of the EPS that produce extreme precipitation could provide information on the potential occurrence of high-impact weather at least five days in advance. Therefore, accurately forecasting the time and location of

cyclone formation (as shown in Fig. 8) may play a secondary role in predicting its impacts in Greece. In this context, the reliable simulation of moisture inflow, which is more closely linked to large-scale circulation, as previously discussed by the EPS members, could be more crucial for impact prediction.

Interestingly, the overlap of extreme precipitation objects among the EPS members might exceed 70% in the area of Thessaly in Greece for a lead time of even 120 hours (Fig. 10c). This percentage is significantly higher than the maximum percentage of overlap between the cyclone objects (Fig. 8c). This suggests that the EPS members have been more consistent in the production of extreme precipitation even if cyclone centres presented a comparably greater spread. For subsequent lead times, the predictability of extreme precipitation strongly increases, showing a high probability for a lead time of 72 hours. Indeed, almost all members predict extreme precipitation off the coast and in the northeastern part of Greece within the eventually flooded area of Thessaly.

When Daniel made landfall and produced impacts on the Libyan coasts, the EPS showed higher predictability, with cyclone objects and associated extreme precipitation being predicted at least five days in advance by several EPS members (Fig. 10d), albeit the location of both cyclone and precipitation objects are still displaced to the southwest compared to the analysis (Figs. 8d and 10d). This comes per the southern displacement of several ensemble member tracks in Fig. 9a. The probability strongly increases at shorter lead times (Figs. 10f and 10h), and all EPS members tend to converge to similar cyclone locations when reaching a lead time of one day (Fig. 8h).

The potential of extreme precipitation leading to substantial socio-economic impacts has also been transferred to hydrologic discharge forecasts. The hydrographs presented in Fig. 11 examine river discharge predictability as forecast by the operational European Flood Awareness System (EFAS) during Daniel. For the Peneus River outlet in Thessaly, the forecast initiated on 1 September underpredicted the peak discharge on 5 September. Nevertheless, extreme river discharges were evident for several members five days in advance. The forecast accuracy improved, getting closer to the event, with ensemble members (grey stripes) converging towards the peak discharge ("perfect forecast" - red line). This trend indicates an increasing reliability of the forecast as the lead time decreases, particularly within 48 hours of the event. The skill in discharge predictability for the Peneus River can be attributed, in part, to the large size of the basin (11.063 km²), which aligns relatively well with the spatial resolution of the EFAS model, enabling an accurate representation of distributed hydrological processes and moderating runoff variability.

The forecasts for the Wadi Derna River outlet (Fig. 11, right panels) exhibit significant variability and fail to converge during the earlier forecast initialization dates and at shorter lead times. This persistent lack of convergence can be attributed to distinct challenges of both temporal scales. For earlier forecast initialization dates, the primary source of variability lies in the westward displacement of extreme precipitation predicted by the EPS (Figs. 10b and 10d). For example, forecasts initialized on 9 September, during a critical period for implementing preventative measures, display a wide spread and a shortfall in the median forecast compared to the benchmark (red line). This variability persists even for forecasts initialized on 10 September. The failure to converge at shorter lead times is compounded by challenges inherent to the Wadi Derna catchment. The resolution of the precipitation forcings used in the forecasts, combined with the relatively small size (575 km²) and flash-flood-prone nature of this basin, amplify the uncertainties in predicting discharge, particularly in response to localized extreme rainfall.

Figure 4 provides critical context by comparing the peak mean daily river discharge during Storm Daniel with the historical baseline. The unprecedented magnitude of the event is evident in Fig. 4b, where river discharges exceeded the historical reanalysis by at least fivefold in certain regions. However, the relatively weak signal for the Wadi Derna catchment underscores the limitations of the GloFAS and EFAS systems in accurately resolving runoff dynamics in smaller basins. This discrepancy is primarily attributed to insufficient model resolution, inaccuracies in rainfall inputs, and the lack of detailed hydrological calibration for these catchments. In contrast, the much stronger

signal observed in the Peneus catchment aligns with larger basin sizes and better-resolved hydrological processes, where models more effectively captured the extreme nature of the event.

The ability of EFAS to predict extreme events, as shown in Fig. 11, highlights its value in forecasting severe hydrological impacts. However, discrepancies in simulated peak discharge remain apparent, such as the overestimation of runoff for the Peneus River outlet. EFAS simulated peak discharge at approximately 5000 m³ s⁻¹, whereas observed values, based on station-level data and H-Q curve estimates, were less than 2000 m³ s⁻¹ (Dimitriou et al, 2024). This overestimation reflects inherent limitations in the model's spatial resolution and hydrological representation. Furthermore, the absence of flood protection infrastructure, such as levees or dams that attenuate runoff and peak flows, is not accounted for in the EFAS and GloFAS systems, contributing to these discrepancies. Additionally, the simplified representation of retention processes, including floodplain storage and wetland buffering, further amplifies discharge estimates in some regions. For smaller basins such as Wadi Derna, the rapid hydrological response to localized extreme rainfall presents additional challenges. The variability in rainfall distribution, coupled with the model's limited ability to capture localized hydrological dynamics, results in a weaker signal for the catchment, even during an event as extreme as Storm Daniel. These limitations emphasize the need for improved model resolution, enhanced precipitation forcings, and better calibration tailored to local catchment characteristics.

Nonetheless, EFAS's ability to predict extreme river discharges, particularly within short lead times, demonstrates the potential of operational forecast systems in capturing the extreme values of such events. Supported by EFAS and GloFAS, the Copernicus Emergency Management Service (CEMS) provides critical insights into the timing and magnitude of extreme hydrological events. These forecasts are vital for enhancing preparedness and response strategies in the face of escalating climate extremes, offering essential tools for civil protection efforts and mitigating the socio-economic impacts of such disasters.

# 5.2 The Role of Natural Variability and human-driven climate change in changing Daniel's dynamics

We use ClimaMeter's analogue-based approach (Faranda et al., 2024) to study the influence of human-driven climate change and natural variability on Storm Daniel. By comparing surface pressure patterns in the periods 1979–2000 ("past") and 2001–present ("current"), we identify how similar Mediterranean depressions have evolved. We use MSWX data to analyze temperature, precipitation, and wind speed changes associated with these analogues. We repeat the analysis twice, once for 5-6 September, when Daniel impacted Greece, and once for 10-11 September, when Daniel impacted Libva.

Regarding the impacts in Greece, we searched for analogues for 5 September 2023 within the region defined within the domain shown in Fig. 12a and within the extended autumn season from September to December (SOND). Figure 12a-d shows that cyclone systems similar to Daniel impacting Greece have the same order of pressure minima in their centre as in the past. Figure 12e-h shows that during depressions, temperatures in the Ionian Sea have increased by approximately 2°C and decreased over Anatolia. Precipitation analysis (Fig. 12j-l) indicates that such events produce heavier rainfall over the Ionian Sea but generally reduced precipitation amounts over continental Greece and the Peloponnese (ranging between 4 and 12 mm day<sup>-1</sup>). To examine potential changes in the dynamical characteristics of these events, the metrics Q, D, and  $\Theta$  are computed and shown in Figs. 12q-s. . These figures reveal no significant differences between the past and present climate periods.. However, metric Q provides insight into the similarity of current events with past analogues, showing that the events have comparable counterparts in both time frames.. Notably, similar events have become more frequent in December, whereas they were previously concentrated in October (Fig. 12t). To assess the potential influence of low-frequency modes of natural variability on the differences observed in the analogue composite maps, we compare the distributions of ENSO, AMO and PDO values on the analogue dates in both the past and present periods and test the statistical significance of the observed differences. For this date, our analysis suggests that natural climate variability, particularly the AMO and PDO, may have influenced the development of the MSLP pattern associated with the storm (Figs. 12u-w).

To clarify the trend in event frequency, Fig. 12x expands the analysis to include 33 analogues for the whole period (1979-2022) instead of 15 in each 20-year period.

We repeat the analysis for 10-11 September 2023 within the region depicted in Fig. 13a, focusing on analogue detection for the SOND period. Results are reported in Fig. 13. The MSLP changes (Fig. 13d) show no substantial differences in the areas significantly affected. The temperature changes (Fig. 13h) indicate warming of up to  $+2^{\circ}$ C over the eastern part of the domain. Precipitation changes (Fig. 13l) show that similar events produced higher precipitation amounts along the eastern Libyan coast (ranging from 5 and 9 mm day<sup>-1</sup>), which experienced intense rainfall from Daniel on 10 September 2023. The metrics Q, D, and  $\Theta$  (Figs. 13q-s) show no significant differences between the past and present periods. Whereas the 5 September analysis of Q identified suitable analogues, in this case, Q shows that no good analogues are available, , underscoring the exceptional nature of Daniel's pressure pattern when the storm impacted Libya. The frequency of such events has decreased in September and November, with a slight increase observed in December (Fig. 13t). As with the 5 September, the AMO and PDO may have influenced the development of the MSLP pattern linked to the storm (Figs. 13u-w). Figure 13x showed changes in event frequency when 30 analogues were considered for the entire period analyzed, instead of 15 in both periods. As in the case of impacts in Greece, a significant increasing trend in frequency is found.

The analogues method helps us understand extreme weather events like Daniel by comparing them to similar past events and seeing how they have changed over time. Our results suggest a role of the AMO and PDO in modulating the large-scale atmospheric patterns conducive to the development of Storm Daniel. Previous studies (see Hodgkins et al. 2017 and references therein) have suggested that positive phases of the AMO can enhance the likelihood of persistent ridges over Europe and modify Mediterranean circulation patterns, while the PDO has been linked to alterations in the waveguide structure of the jet stream across the Northern Hemisphere. These teleconnections may precondition the synoptic environment in which Mediterranean cyclones form and evolve, as Maslova et al. (2017) suggested. This assessment is exploratory, highlighting potential associations without making definitive attributions given the limitations of a 40-year dataset.

For 5 September, when Daniel impacted Greece, we found similar past Mediterranean storms, suggesting that this part of the storm's track was unusual but not unprecedented. Since we see no major changes in the MSLP pattern, the increase in precipitation over the region is most likely linked to higher SSTs, which provide more moisture to the atmosphere. This matches other studies that show Greece experienced extreme moisture anomalies.

For 10-11 September, when Daniel reached Libya, our method found no suitable past matches, highlighting the exceptional nature of the storm's pressure pattern at this stage. However, like in Greece, we do not see substantial changes in MSLP. The increased frequency of circulation analogues to Storm Daniel in recent decades suggests that the synoptic conditions conducive to such extreme Mediterranean cyclones are becoming more common. This shift implies a heightened background risk for similar high-impact events under present-day climate conditions. Combining multiple lines of evidence, as customary in attribution studies, we can deduce that the increase in rainfall over Libya was likely driven by warmer SSTs and a warmer atmosphere, which can hold more water (Clausius-Clapeyron relationship) rather than a shift in atmospheric dynamics patterns. The MSWX dataset provides a reliable representation of large-scale atmospheric patterns but does not fully capture localized extreme precipitation intensities, which explains why our figures underestimate the observed rainfall totals, particularly in Libya; therefore, our analysis should be interpreted as reflecting broader climatological trends rather than exact station-level extremes. We also acknowledge that the smallscale, Medicane structure of storm Daniel presents significant challenges for attribution studies based on relatively coarse-resolution reanalyses. In this study, we do not attempt to reproduce the mesoscale features or rapid intensification processes that characterized Daniel. Instead, our analysis focuses on the large-scale circulation patterns that may create a favorable environment for developing such compact systems. While this approach provides insights into the changing likelihood of conducive synoptic configurations under current climate conditions, it is important to note that critical aspects of

Daniel's intensity and structure may be underrepresented in our framework. As such, our results should be interpreted as exploratory and limited by the resolution and scope of the datasets employed. Importantly, while Daniel brought heavy rainfall, the disaster in Derna was mainly caused by the failure of poorly maintained dams (Shirzaei et al., 2025). Dente et al. (2024) confirm this, showing that while rainfall was intense, it was not so extreme to explain the scale of destruction—factors like unsafe building locations and poor emergency response played a major role. These considerations underscore a key point: while climate change can amplify precipitation by increasing SSTs, the most severe impacts often depend on societal factors such as infrastructure resilience and disaster preparedness.

## 6. Summary and conclusions

In the last decade, more than 410,000 deaths have been attributed to weather-related disasters, mostly in low-income countries where heatwaves and intense precipitation events are the leading causes of death. Besides fatalities, 1.7 billion people have been affected in the 2010-2020 decade by these kinds of phenomena. The IFRC World Disasters Report (2020) concluded that climate change is a risk multiplier, i.e., intensifying existing vulnerabilities, particularly in low-income countries. A glaring example of the impact of such disasters is the recent floods in the Mediterranean, especially in Greece and Libya, following the Mediterranean cyclone Daniel.

This study aimed to comprehensively analyze Medicane Daniel by linking atmospheric dynamics, predictability, and impacts. Impacts—including flooding and coastal sea-state conditions in Libya—were also evaluated with numerical weather prediction models. We placed these findings in a broader climatological context of cyclone-driven precipitation, underscoring how the observed impacts connect to climate-change attribution for both catastrophic events.

From the perspective of atmospheric dynamics, the processes governing Daniel's development were similar to those identified for other intense Mediterranean cyclones: cyclogenesis was triggered by the intrusion of an upper-level PV streamer in the Ionian Sea, and thereafter, the cyclone propagated erratically southwards, then turned towards the east on 8 September, and then developed into a well defined mesoscale tropical-like cyclonic system. Regarding impacts, we identified two distinct stages: the first is relevant to cyclogenesis, where Daniel had newly formed and affected Greece with severe floods (on 5 September 2023). In the second stage, Daniel reached maturity after making landfall in Libya, where it inflicted severe socio-economic impacts on 11 September 2023 due to floods (about 5 days after the floods in Greece). Storm Daniel produced extreme precipitation during both stages by transporting moist air toward the flood-affected regions. The moisture transport followed the large-scale atmospheric circulation and drew on two primary sources: an anomalously warm Mediterranean Sea and the continental areas of central and eastern Europe. Together, these reservoirs supplied the water vapor that fueled the catastrophic rainfall.

In Greece, the floods occurred during the cyclogenesis stage in regions quite remote from the cyclone centre. On the other hand, floods in Libya occurred close to the cyclone centre and at the stage of its maximum intensity. During its first stage in Greece, the predictions of the cyclone formation were relatively poor for lead times of more than four days. It was a rather challenging issue for the ECMWF EPS to forecast precisely the intrusion of the PV streamer in the Mediterranean. This result aligns with previous studies that showed relatively poor performance in predicting medicane occurrences for lead times of four to five days (Di Muzio et al., 2019). With higher confidence, the ECMWF EPS could forecast cyclogenesis, and thus the flooding event, for shorter lead times.

During its second stage (impacts in Libya), the cyclone transitioned into a medicane, making landfall in Libya within a few days after its formation. The predictions of the medicane track -and therefore its landfall- showed higher certainty for lead times of four days. These results indicate that numerical weather-prediction models are less skillful at predicting cyclogenesis; however, once the cyclone has formed, the models could become more reliable at forecasting its subsequent track.

Precipitation amounts were found to correspond to climate extremes in both countries, Greece and Libya, where river discharges were responsible for floods that largely exceeded the climatological

maxima of the last 20 years. The numerical weather prediction model could forecast these climate extremes (even if thresholds were defined by reanalysis and not by the same forecast model). This underscores the exceptional potential to give the public timely, accurate warnings about the severity of impending high-impact weather events. In this context, we have analyzed Daniel concerning climate change and provided the means to interpret Daniel as an event whose characteristics can largely be ascribed to human-driven climate change. In these regards, we have performed an analysis based on analogues; indeed, several cyclones with similar characteristics were found during winter. The anomalous occurrence of such a storm in September, a warmer month for SST, could be a reason for enhancing its destructiveness through enhanced precipitation.

In the scientific literature, weather events are typically analysed as case studies with specific objectives that rarely escape the narrow scope of a single scientific discipline. Here, we used Daniel, a high-impact weather event, as a centrepiece of different approaches to better understand socioeconomic impacts through the prism of both weather and climate scales. We find such an approach valuable for linking different scientific communities and essential for communicating hazards to the local population. We envisage using this interdisciplinary approach for other weather

#### Acknowledgements

extremes and regions.

We gratefully acknowledge Ambrogio Volontè and an anonymous reviewer for accurately reviewing our paper. This article is based upon collaborative work of two COST Actions: CA19109 "MedCyclones" and CA22162 "FutureMed", supported by COST – European Cooperation in Science and Technology (http://www.cost.eu, last access: 14 February 2025) and from project "Earth Observations as a cornerstone to the understanding and prediction of tropical like cyclone risk in the Mediterranean (MEDICANES)", ESA Contract No. 4000144111/23/I-KE. Georgios Kyros from the National Observatory of Athens/meteo.gr is acknowledged for helping collect the Copernicus Sentinel-2 data in Figure 1. The Israel Science Foundation (grant \#978/23) funds AH's contribution. PP was funded by the EU's Horizon Europe program, OCEANIDS (G.A. No. 101112919). SD acknowledges the support from Next Generation EU, Mission 4, Component 1, CUP B53D23007490006, project "Exploring Atmospheric Rivers in the Mediterranean and their connection with extreme hydrometeorological events over Italy: observation, modelling and impacts (ARMEX)".; MMM acknowledges financial support from Next Generation EU, Mission 4, Component 1, CUP B53D23007360006, project "Thunderstorm outflows measurements and modeling for strong WIND nowcast and RISK mitigation (WIND RISK)". We thank Franziska Aemisegger for providing the msd-cpp code for the calculation of the moisture sources.

#### **Author contribution**

EF conceptualized this work and coordinated the collection of manuscript content from all coauthors. Stavros Dafis, Silvio Davolio, AH, MMM, FP, KH, and PP contributed input on the meteorological background of the event, discussed atmospheric dynamics and forecast implications, and wrote the relevant sections of the text. MS provided data for the analysis of water sources, which was analyzed by IT. AK and CF contributed data and analyses and wrote the sections on flooding and sea-state, respectively. Finally, DF provided expertise and conducted the analysis of Storm Daniel in the context of climate change attribution.

# **Competing interests**

Silvio Davolio is a member of the editorial board of Weather and Climate Dynamics.

## 7. References

Argüeso, D., Marcos, M. and Amores, A.: Storm Daniel fueled by anomalously high sea surface temperatures in the Mediterranean, npj Clim Atmos Sci 7, 307, https://doi.org/10.1038/s41612-024-00872-2, 2024.

- 870 Avolio, E., Fanelli, C., Pisano, A. and Miglietta, M. M.: Unveiling the relationship between
- 871 Mediterranean tropical-like cyclones and rising Sea Surface Temperature. Geophysical Research
- 872 Letters 51, e2024GL109921, https://doi.org/10.1029/2024GL109921, 2024.

- Beck, H. E., Van Dijk, A. I. J. M., Larraondo, P. R., McVicar, T. R., Pan, M., Dutra, E., and Miralles,
- 875 D. G.: MSWX: Global 3-Hourly 0.1° Bias-Corrected Meteorological Data Including Near-Real-Time
- Updates and Forecast Ensembles, Bulletin of the American Meteorological Society, 103, E710–E732,
- 877 https://doi.org/10.1175/BAMS-D-21-0145.1, 2022.

878

Bouin, M.-N. and Lebeaupin Brossier, C.: Impact of a medicane on the oceanic surface layer from a coupled, kilometre-scale simulation, Ocean Sci., 16, 1125–1142, https://doi.org/10.5194/os-16-1125-2020, 2020.

882

Catto, J. L. and Dowdy, A.: Understanding compound hazards from a weather system perspective, Weather and Climate Extremes, 32, 100313, https://doi.org/10.1016/j.wace.2021.100313, 2021.

885

Chaboureau, J., Pantillon, F., Lambert, D., Richard, E., and Claud, C.: Tropical transition of a Mediterranean storm by jet crossing, Quart J Royal Meteoro Soc, 138, 596–611, https://doi.org/10.1002/qj.960, 2012.

889

890 Couto, F. T., Kartsios, S., Lacroix, M., and Andrade, H. N.: A Quick Look at the Atmospheric 891 Circulation Leading to Extreme Weather Phenomena on a Continental Scale, Atmosphere, 15, 1205, https://doi.org/10.3390/atmos15101205, 2024.

893

Davolio, S., Della Fera, S., Laviola, S., Miglietta, M. M., and Levizzani, V.: Heavy Precipitation over Italy from the Mediterranean Storm "Vaia" in October 2018: Assessing the Role of an Atmospheric River, Monthly Weather Review, 148, 3571–3588, https://doi.org/10.1175/MWR-D-20-0021.1, 2020.

897

De Vries, A. J.: A global climatological perspective on the importance of Rossby wave breaking and intense moisture transport for extreme precipitation events, Weather Clim. Dynam., 2, 129–161, https://doi.org/10.5194/wcd-2-129-2021, 2021.

901

Dente, E., Armon, M., and Shmilovitz, Y.: The September 2023 flood in Derna, Libya: an extreme weather event or man-made disaster?, EGU General Assembly 2024, Vienna, Austria, 14–19 Apr 2024, EGU24-15755, https://doi.org/10.5194/egusphere-egu24-15755, 2024.

906 Di Muzio, E., Riemer, M., Fink, A. H., and Maier-Gerber, M.: Assessing the predictability of Medicanes in ECMWF ensemble forecasts using an object-based approach, Quart J Royal Meteoro Soc, 145, 1202–1217, https://doi.org/10.1002/qj.3489, 2019.

909

Dimitriou, E., Efstratiadis, A., Zotou, I., Papadopoulos, A., Iliopoulou, T., Sakki, G.-K., Mazi, K.,
Rozos, E., Koukouvinos, A., Koussis, A. D., Mamassis, N., and Koutsoyiannis, D.: Post-Analysis of
Daniel Extreme Flood Event in Thessaly, Central Greece: Practical Lessons and the Value of State-ofthe-Art Water-Monitoring Networks, Water, 16, 980, https://doi.org/10.3390/w16070980, 2024.

914

915 Faranda, D., Messori, G., and Yiou, P.: Dynamical proxies of North Atlantic predictability and extremes, Sci Rep, 7, 41278, https://doi.org/10.1038/srep41278, 2017.

917

Faranda, D., Bourdin, S., Ginesta, M., Krouma, M., Noyelle, R., Pons, F., Yiou, P., and Messori, G.:
A climate-change attribution retrospective of some impactful weather extremes of 2021, Weather
Clim. Dynam., 3, 1311–1340, https://doi.org/10.5194/wcd-3-1311-2022, 2022.

- Faranda, D., Ginesta, M., Alberti, T., Coppola, E., and Anzidei, M.: Attributing Venice Acqua Alta events to a changing climate and evaluating the efficacy of MoSE adaptation strategy, npj Clim
- 924 Atmos Sci, 6, 181, https://doi.org/10.1038/s41612-023-00513-0, 2023a.

Faranda, D., Messori, G., Coppola, E., Alberti, T., Vrac, M., Pons, F., Yiou, P., Saint Lu, M., Hisi, A.
N. S., Brockmann, P., Dafis, S., Mengaldo, G., and Vautard, R.: ClimaMeter: contextualizing extreme
weather in a changing climate, Weather Clim. Dynam., 5, 959–983, https://doi.org/10.5194/wcd-5-

929 959-2024, 2024.

930

931 Ferrarin, C., Pantillon, F., Davolio, S., Bajo, M., Miglietta, M. M., Avolio, E., Carrió, D. S., Pytharoulis, I., Sanchez, C., Patlakas, P., González-Alemán, J. J., and Flaounas, E.: Assessing the coastal hazard of Medicane Ianos through ensemble modelling, Nat. Hazards Earth Syst. Sci., 23, 2273–2287, https://doi.org/10.5194/nhess-23-2273-2023, 2023a.

935

936 Ferrarin, C., Orlić, M., Bajo, M., Davolio, S., Umgiesser, G., and Lionello, P.: The contribution of a mesoscale cyclone and associated meteotsunami to the exceptional flood in Venice on November 12, 2019, Quart J Royal Meteoro Soc, 149, 2929–2942, https://doi.org/10.1002/qj.4539, 2023b.

939

940 Flaounas, E., Raveh-Rubin, S., Wernli, H., Drobinski, P., and Bastin, S.: The dynamical structure of intense Mediterranean cyclones, Clim Dyn, 44, 2411–2427, https://doi.org/10.1007/s00382-014-2330-2, 2015.

943

944 Flaounas, E., Di Luca, A., Drobinski, P., Mailler, S., Arsouze, T., Bastin, S., Beranger, K., and 945 Lebeaupin Brossier, C.: Cyclone contribution to the Mediterranean Sea water budget, Clim Dyn, 46, 946 913–927, https://doi.org/10.1007/s00382-015-2622-1, 2016.

947

948 Flaounas, E., Kotroni, V., Lagouvardos, K., Gray, S. L., Rysman, J.-F., and Claud, C.: Heavy rainfall 949 in Mediterranean cyclones. Part I: contribution of deep convection and warm conveyor belt, Clim 950 Dyn, 50, 2935–2949, https://doi.org/10.1007/s00382-017-3783-x, 2018.

951

Flaounas, E., Fita, L., Lagouvardos, K., and Kotroni, V.: Heavy rainfall in Mediterranean cyclones, Part II: Water budget, precipitation efficiency and remote water sources, Clim Dyn, 53, 2539–2555, https://doi.org/10.1007/s00382-019-04639-x, 2019.

955

956 Flaounas, E., Gray, S. L., and Teubler, F.: A process-based anatomy of Mediterranean cyclones: from baroclinic lows to tropical-like systems, Weather Clim. Dynam., 2, 255–279, 958 https://doi.org/10.5194/wcd-2-255-2021, 2021.

959

Flaounas, E., Davolio, S., Raveh-Rubin, S., Pantillon, F., Miglietta, M. M., Gaertner, M. A., Hatzaki,
M., Homar, V., Khodayar, S., Korres, G., Kotroni, V., Kushta, J., Reale, M., and Ricard, D.:
Mediterranean cyclones: current knowledge and open questions on dynamics, prediction, climatology
and impacts, Weather Clim. Dynam., 3, 173–208, https://doi.org/10.5194/wcd-3-173-2022, 2022.

964

Flaounas, E., Aragão, L., Bernini, L., Dafis, S., Doiteau, B., Flocas, H., Gray, S. L., Karwat, A., Kouroutzoglou, J., Lionello, P., Miglietta, M. M., Pantillon, F., Pasquero, C., Patlakas, P., Picornell, M. Á., Porcù, F., Priestley, M. D. K., Reale, M., Roberts, M. J., Saaroni, H., Sandler, D., Scoccimarro, E., Sprenger, M., and Ziv, B.: A composite approach to produce reference datasets for extratropical cyclone tracks: application to Mediterranean cyclones, Weather Clim. Dynam., 4, 639–661, https://doi.org/10.5194/wcd-4-639-2023, 2023.

971

Grimaldi, S., Salamon, P., Disperati, J., Zsoter, E., Russo, C., Ramos, A., Carton De Wiart, C., Barnard, C., Hansford, E., Gomes, G., Prudhomme, C. (2022): River discharge and related historical data from the Global Flood Awareness System. v4.0. European Commission, Joint Research Centre (JRC). URL: https://cds.climate.copernicus.eu/cdsapp#!/dataset/cems-glofas-historical (Accessed on 09-Oct-2023)

977

978 Global Data Institute of the UN International Organization for Migration (IOM). 2023. Libya — 979 Storm Daniel Flash update 8 (13 October 2023)

981 He, K., Yang, Q., Shen, X., Dimitriou, E., Mentzafou, A., Papadaki, C., Stoumboudi, M., and 982 Anagnostou, E. N.: Brief communication: Storm Daniel Flood Impact in Greece 2023: Mapping Crop 983 and Livestock Exposure from SAR, https://doi.org/10.5194/nhess-2023-173, 12 October 2023.

984

985 Hersbach, H., Bell, B., Berrisford, P., Hirahara, S., Horányi, A., Muñoz-Sabater, J., Nicolas, J., 986 Peubey, C., Radu, R., Schepers, D., Simmons, A., Soci, C., Abdalla, S., Abellan, X., Balsamo, G., 987 Bechtold, P., Biavati, G., Bidlot, J., Bonavita, M., De Chiara, G., Dahlgren, P., Dee, D., Diamantakis, 988 M., Dragani, R., Flemming, J., Forbes, R., Fuentes, M., Geer, A., Haimberger, L., Healy, S., Hogan, 989 R. J., Hólm, E., Janisková, M., Keeley, S., Laloyaux, P., Lopez, P., Lupu, C., Radnoti, G., De Rosnay, 990 P., Rozum, I., Vamborg, F., Villaume, S., and Thépaut, J.: The ERA5 global reanalysis, Quart J Royal Meteoro Soc, 146, 1999–2049, https://doi.org/10.1002/qj.3803, 2020.

991

992

993 Hewson, T., Ashoor, A., Boussetta, S., Emanuel, K., Lagouvardos, K., Lavers, D., Magnusson, L., 994 Pillosu, F., Zsoter, E., Medicane Daniel: an extraordinary cyclone with devastating impacts, ECMWF 995 newsletters 179, 2024, 33-47.

996

997 Hochman, A., Scher, S., Quinting, J., Pinto, J. G., and Messori, G.: Dynamics and predictability of 998 Mediterranean, Clim 2047-2064, the Eastern Dyn, 58, 999 https://doi.org/10.1007/s00382-020-05465-2, 2022a.

1000

1001 Hochman, A., Marra, F., Messori, G., Pinto, J. G., Raveh-Rubin, S., Yosef, Y., and Zittis, G.: Extreme 1002 weather and societal impacts in the eastern Mediterranean, Earth Syst. Dynam., 13, 749–777, 1003 https://doi.org/10.5194/esd-13-749-2022, 2022b.

1004

1005 Hochman, A., Plotnik, T., Marra, F., Shehter, E.-R., Raveh-Rubin, S., and Magaritz-Ronen, L.: The 1006 sources of extreme precipitation predictability; the case of the 'Wet' Red Sea Trough, Weather and 1007 Climate Extremes, 40, 100564, https://doi.org/10.1016/j.wace.2023.100564, 2023.

1008

1009 Hochman, A., Shachar, N., and Gildor, H.: Unraveling sub-seasonal precipitation variability in the 1010 East via Indian Ocean sea surface temperature. Sci Rep. 1011 https://doi.org/10.1038/s41598-024-53677-x, 2024.

1012

1013 Hodgkins, G. A., Whitfield, P. H., Burn, D. H., Hannaford, J., Renard, B., Stahl, K., ... & Wilson, D. 1014 (2017). Climate-driven variability in the occurrence of major floods across North America and 1015 Europe. Journal of Hydrology, 552, 704-717.

1016

1017 IFRC (International Federation of Red Cross and Red Crescent Societies). World Disasters Report 1018 2020 Executive Summary. https://www.ifrc.org/document/world-disasters-report-2020

1019

1020 Khodayar, S., Davolio, S., Di Girolamo, P., Lebeaupin Brossier, C., Flaounas, E., Fourrie, N., Lee, 1021 K.-O., Ricard, D., Vie, B., Bouttier, F., Caldas-Alvarez, A., and Ducrocq, V.: Overview towards 1022 improved understanding of the mechanisms leading to heavy precipitation in the western 1023 Mediterranean: lessons learned from HyMeX, Atmos. Chem. Phys., 21, 17051–17078, 1024 https://doi.org/10.5194/acp-21-17051-2021, 2021.

1025

1026 Khodayar, S., Kushta, J., Catto, J. L., Dafis, S., Davolio, S., Ferrarin, C., Flaounas, E., Groenemeijer, 1027 P., Hatzaki, M., Hochman, A., Kotroni, V., Landa, J., Láng-Ritter, I., Lazoglou, G., Liberato, M. L. 1028 R., Miglietta, M. M., Papagiannaki, K., Patlakas, P., Stojanov, R., and Zittis, G.: Mediterranean 1029 Cyclones in a Changing Climate: A Review on Their Socio-Economic Impacts, Reviews of 1030 Geophysics, 63, e2024RG000853, https://doi.org/10.1029/2024RG000853, 2025.

1031

1032 Korres, G., Ravdas, M., Denaxa, D., & Sotiropoulou, M. (2021). Mediterranean Sea Waves 1033 Reanalysis INTERIM (CMEMS Med-Waves, MedWAM3I system) (Version 1) [Data set].

- 1034 Copernicus Monitoring Environment Marine Service (CMEMS).
- 1035 https://doi.org/10.25423/CMCC/MEDSEA\_MULTIYEAR\_WAV\_006\_012\_MEDWAM3I

- 1037 Korres, G., Oikonomou, C., Denaxa, D., & Sotiropoulou, M. (2023). Mediterranean Sea Waves
- 1038 Analysis and Forecast (Copernicus Marine Service MED-Waves, MEDWAM4 system) (Version 1)
- 1039 [Data set]. Copernicus Marine Service (CMS).
- 1040 https://doi.org/10.25423/CMCC/MEDSEA ANALYSISFORECAST WAV 006 017 MEDWAM4

1041

- 1042 Lagouvardos, K., Kotroni, V., Bezes, A., Koletsis, I., Kopania, T., Lykoudis, S., Mazarakis, N.,
- 1043 Papagiannaki, K., and Vougioukas, S.: The automatic weather stations NOANN network of the
- 1044 National Observatory of Athens: operation and database, Geoscience Data Journal, 4, 4–16,
- 1045 https://doi.org/10.1002/gdj3.44, 2017.
- 1046 Maslova, V., Voskresenskaya, E. N., & Lubkov, A. (2017). Multidecadal change of winter cyclonic
- 1047 activity in the Mediterranean associated with AMO and PDO. Terrestrial, Atmospheric and Oceanic
- 1048 *Sciences*, 28(6), 965–977. https://doi.org/10.3319/TAO.2017.04.23.01

1049

- 1050 Messmer, M., Gómez-Navarro, J. J., and Raible, C. C.: Sensitivity experiments on the response of Vb
- 1051 cyclones to sea surface temperature and soil moisture changes, Earth Syst. Dynam., 8, 477–493,
- 1052 https://doi.org/10.5194/esd-8-477-2017, 2017.

1053

- 1054 Miglietta, M. M., Moscatello, A., Conte, D., Mannarini, G., Lacorata, G., and Rotunno, R.: Numerical
- analysis of a Mediterranean 'hurricane' over south-eastern Italy: Sensitivity experiments to sea
- 1056 surface temperature, Atmospheric Research, 101, 412–426,
- 1057 https://doi.org/10.1016/j.atmosres.2011.04.006, 2011.

1058

- 1059 Miglietta, M. M., Carnevale, D., Levizzani, V., and Rotunno, R.: Role of moist and dry air advection
- in the development of Mediterranean tropical-like cyclones (medicanes), Quart J Royal Meteoro Soc,
- 1061 147, 876–899, https://doi.org/10.1002/qj.3951, 2021.

1062

- 1063 Miglietta M. M., González-Alemán J. J., Panegrossi G., Gaertner M. A., Pantillon F., Pasquero C.,
- 1064 Schultz D. M., D'Adderio L. P., Dafis S., Husson R., Ricchi A., Carrió D. S., Davolio S., Fita L.,
- 1065 Picornell M. A., Pytharoulis I., Raveh-Rubin S., Scoccimarro E., Bernini L., Cavicchia L., Conte D.,
- 1066 Ferretti R., Flocas H., Gutiérrez-Fernández J., Hatzaki M., Homar Santaner V., Jansà A., Patlakas P.,
- 1067 Flaounas E., Defining Medicanes: Bridging the Knowledge Gap Between Tropical and Extratropical
- 1068 Cyclones in the Mediterranean, Bull. Am. Meteor. Soc., submitted

1069

- 1070 Nissen, K. M., Leckebusch, G. C., Pinto, J. G., Renggli, D., Ulbrich, S., and Ulbrich, U.: Cyclones
- 1071 causing wind storms in the Mediterranean: characteristics, trends and links to large-scale patterns,
- 1072 Nat. Hazards Earth Syst. Sci., 10, 1379–1391, https://doi.org/10.5194/nhess-10-1379-2010, 2010.

1073

- 1074 Pantillon, F. P., Chaboureau, J.-P., Mascart, P. J., and Lac, C.: Predictability of a Mediterranean
- 1075 Tropical-Like Storm Downstream of the Extratropical Transition of Hurricane Helene (2006),
- 1076 Monthly Weather Review, 141, 1943–1962, https://doi.org/10.1175/MWR-D-12-00164.1, 2013.

1077

- 1078 Pantillon, F., Davolio, S., Avolio, E., Calvo-Sancho, C., Carrió, D. S., Dafis, S., Gentile, E. S.,
- 1079 Gonzalez-Aleman, J. J., Gray, S., Miglietta, M. M., Patlakas, P., Pytharoulis, I., Ricard, D., Ricchi,
- 1080 A., Sanchez, C., and Flaounas, E.: The crucial representation of deep convection for the cyclogenesis
- 1081 of Medicane Ianos, Weather Clim. Dynam., 5, 1187–1205, https://doi.org/10.5194/wcd-5-1187-2024,
- 1082 2024.

1083

- 1084 Patlakas, P., Stathopoulos, C., Tsalis, C., and Kallos, G.: Wind and wave extremes associated with
- 1085 tropical-like cyclones in the Mediterranean basin, Intl Journal of Climatology, 41,
- 1086 https://doi.org/10.1002/joc.6795, 2021.

Pfahl, S. and Wernli, H.: Quantifying the Relevance of Cyclones for Precipitation Extremes, Journal of Climate, 25, 6770–6780, https://doi.org/10.1175/JCLI-D-11-00705.1, 2012.

1090

Portal, A., Raveh-Rubin, S., Catto, J. L., Givon, Y., and Martius, O.: Linking compound weather extremes to Mediterranean cyclones, fronts, and airstreams, Weather Clim. Dynam., 5, 1043–1060, https://doi.org/10.5194/wcd-5-1043-2024, 2024.

1094

Pytharoulis, I.: Analysis of a Mediterranean tropical-like cyclone and its sensitivity to the sea surface temperatures, Atmospheric Research, 208, 167–179, https://doi.org/10.1016/j.atmosres.2017.08.009, 2018.

1098

1099 Qiu J., Zhao W., Brocca L., Paolo Tarolli (2023). Storm Daniel revealed the fragility of the 1100 Mediterranean region. The Innovation Geoscience 1(3), 100036. https://doi.org/10.59717/j.xinn-1101 geo.2023.100036

1102

1103 Raveh-Rubin, S. and Flaounas, E.: A dynamical link between deep Atlantic extratropical cyclones and 1104 intense Mediterranean cyclones, Atmospheric Science Letters, 18, 215–221, 1105 https://doi.org/10.1002/asl.745, 2017.

1106

Raveh-Rubin, S. and Wernli, H.: Large-scale wind and precipitation extremes in the Mediterranean: dynamical aspects of five selected cyclone events, Quart J Royal Meteoro Soc, 142, 3097–3114, https://doi.org/10.1002/qj.2891, 2016.

1110

- 1111 Reale, M., Cabos Narvaez, W. D., Cavicchia, L., Conte, D., Coppola, E., Flaounas, E., Giorgi, F.,
  1112 Gualdi, S., Hochman, A., Li, L., Lionello, P., Podrascanin, Z., Salon, S., Sanchez-Gomez, E.,
  1113 Scoccimarro, E., Sein, D. V., and Somot, S.: Future projections of Mediterranean cyclone
  1114 characteristics using the Med-CORDEX ensemble of coupled regional climate system models, Clim
- 1115 Dyn, 58, 2501–2524, https://doi.org/10.1007/s00382-021-06018-x, 2022.

1116

1117 Ricchi, A.,Miglietta, M. M., Barbariol, F., Benetazzo, A., Bergamasco, A., Bonaldo, D., Cassardo, C., 1118 Falcieri, F. M., Modugno, G., Russo, A., Sclavo, M., and Carniel, S.: Sensitivity of a Mediterranean 1119 tropical-like cyclone to different model configurations and coupling strategies, Atmosphere, 8, 1–32, https://doi.org/10.3390/atmos8050092, 2017.

1121

1122 Romaniello, V., Oddo, P., Tonani, M., Torrisi, L., Grandi, A., and Pinardi, N.: Impact of Sea Surface 1123 Temperature on COSMO Forecasts of a Medicane over the Western Mediterranean Sea, JEASE, 5, 1124 https://doi.org/10.17265/2159-581X/2015.06.002, 2015.

1125

1126 Romero, R. and Emanuel, K.: Climate Change and Hurricane-Like Extratropical Cyclones: 1127 Projections for North Atlantic Polar Lows and Medicanes Based on CMIP5 Models, J. Climate, 30, 1128 279–299, https://doi.org/10.1175/JCLI-D-16-0255.1, 2017.

1129

1130 Rousseau-Rizzi, R., Raveh-Rubin, S., Catto, J. L., Portal, A., Givon, Y., and Martius, O.: A storm-relative climatology of compound hazards in Mediterranean cyclones, Weather Clim. Dynam., 5, 1079–1101, https://doi.org/10.5194/wcd-5-1079-2024, 2024.

1133

Sanchez, C., Gray, S., Volonte', A., Pantillon, F., Berthou, S., and Davolio, S.: The impact of preceding convection on the development of Medicane Ianos and the sensitivity to sea surface temperature. Weather Clim. Dynam., 5, 1429 - 1455, https://doi.org/10.5194/wcd-5-1429-2024, 2024.

1137

Sandler, D., Saaroni, H., Ziv, B., Hochman, A., Harnik, N., and Rostkier-Edelstein, D.: A multiscale approach to statistical downscaling of daily precipitation: Israel as a test case, Intl Journal of Climatology, 44, 59–71, https://doi.org/10.1002/joc.8315, 2024.

- 1142 Scherrmann, A., Wernli, H., and Flaounas, E.: The upstream–downstream connection of North
- 1143 Atlantic and Mediterranean cyclones in semi-idealized simulations, Weather Clim. Dynam., 5, 419–
- 1144 438, https://doi.org/10.5194/wcd-5-419-2024, 2024.

- 1146 Shirzaei, M., Vahedifard, F., Sadhasivam, N., Ohenhen, L., Dasho, O., Tiwari, A., Werth, S., Azhar,
- 1147 M., Zhao, Y., Nicholls, R. J., and AghaKouchak, A.: Aging dams, political instability, poor human
- 1148 decisions and climate change: recipe for human disaster, npj Nat. Hazards, 2, 1–8,
- 1149 https://doi.org/10.1038/s44304-024-00056-1, 2025.

1150

- 1151 Sioni, F., Davolio, S., Grazzini, F., and Giovannini, L.: Revisiting the atmospheric dynamics of the
- 1152 two century floods over north-eastern Italy. Atmos. Research, 286, 106662,
- 1153 https://doi.org/10.1016/j.atmosres.2023.106662, 2023.

1154

- 1155 Sodemann, H., Schwierz, C., and Wernli, H.: Interannual variability of Greenland winter precipitation
- sources: Lagrangian moisture diagnostic and North Atlantic Oscillation influence, J. Geophys. Res.,
- 1157 113, 2007JD008503, https://doi.org/10.1029/2007JD008503, 2008.

1158

- 1159 Sprenger, M. and Wernli, H.: The LAGRANTO Lagrangian analysis tool version 2.0, Geosci.
- 1160 Model Dev., 8, 2569–2586, https://doi.org/10.5194/gmd-8-2569-2015, 2015.

1161

1162 UNICEF. 2023. Libya Storm Daniel & Flooding, Situation Report #1. (14-09-2023)

1163

- 1164 United Nations Office for the Coordination of Humanitarian Affairs (OCHA). 2023. Flash Appeal
- 1165 Libya.

1166

- 1167 Varlas, G., Vervatis, V., Spyrou, C., Papadopoulou, E., Papadopoulos, A., and Katsafados, P.:
- 1168 Investigating the impact of atmosphere—wave—ocean interactions on a Mediterranean tropical-like
- 1169 cyclone, Ocean Model., 153, 101675, https://doi.org/10.1016/j.ocemod.2020.101675, 2020.

1170 1171

- 1172 World Meteorological Organisation: https://wmo.int/media/news/libya-floods-show-need-multi-
- hazard-early-warnings-unified-response, 2023a, last access: 10 March 2024.

1174

- 1175 World Meteorological Organisation: https://wmo.int/media/news/storm-daniel-leads-extreme-rain-
- and-floods-mediterranean-heavy-loss-of-life-libya, 2023b, last access: 3 February, 2025

1177

- 1178 Wernli, H. and Davies, H. C.: A Lagrangian-based analysis of extratropical cyclones. I: The method
- 1179 and some applications, Quart J Royal Meteoro Soc, 123, 467–489,
- 1180 https://doi.org/10.1002/qj.49712353811, 1997.

1181

- 1182 World Bank, 2023. Libya Storm and Flooding 2023. Rapid Damage and Needs Assessment.
- 1183 Washington, DC: World Bank, http://recovery.preventionweb.net/quick/82808.

- 1186
- 1187
- 1188
- 1189
- 1190 1191
- 1192
- 1193
- 1194
- 1195
- 1196

## **Figures**

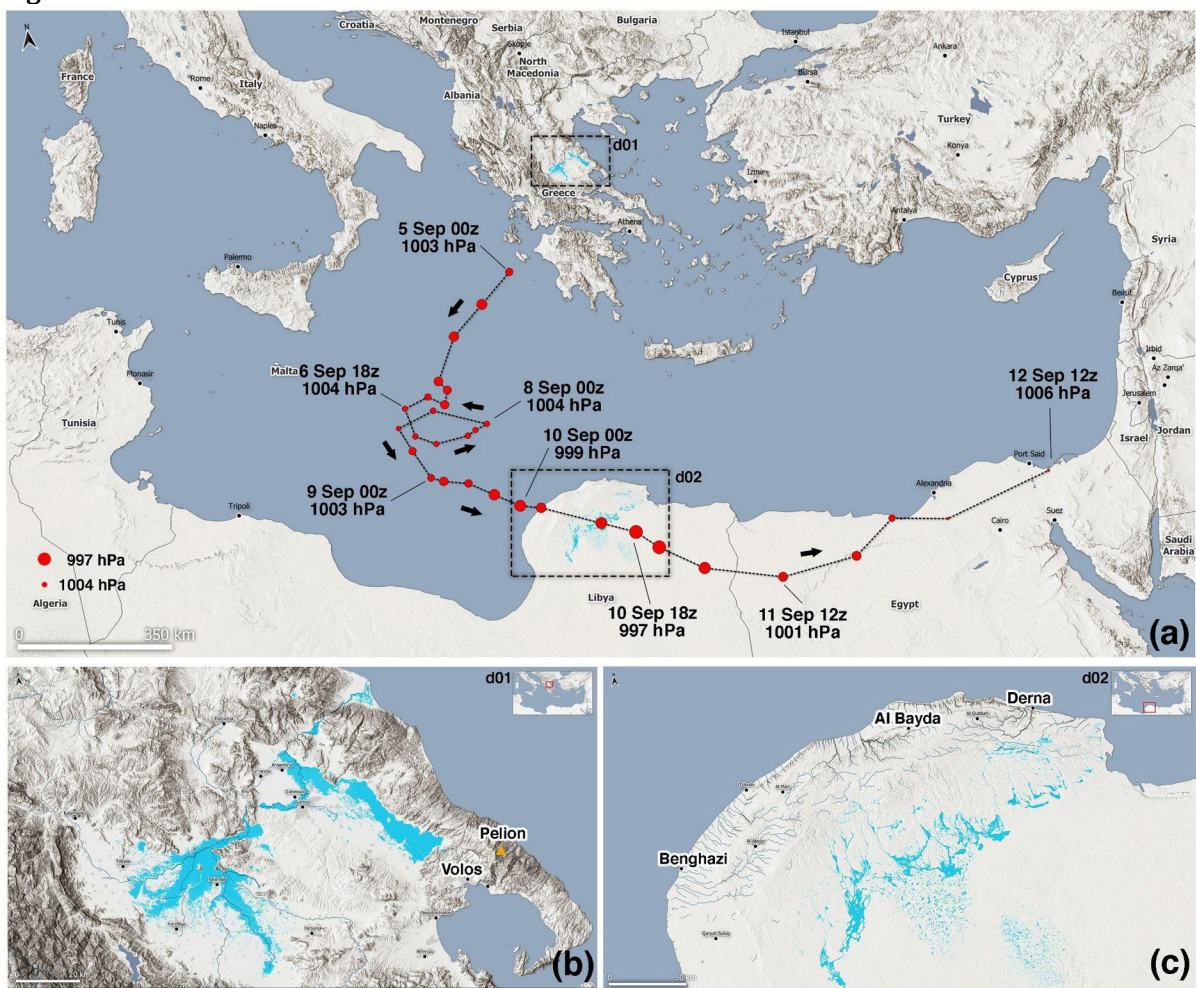


**Figure 1 (a)** Track of Storm Daniel at six-hour intervals based on ECMWF analysis, where the size of red dots is proportional to cyclone depth in terms of minimum MSLP. Flooded areas are shown in cyan and blue tones (acquired by one of the Copernicus Sentinel-2 satellites on 10 and 12 September 2023). Panels **(b)** and **(c)** zoom over central Greece and Libya (square boxes d01 and d02 in panel **a**).

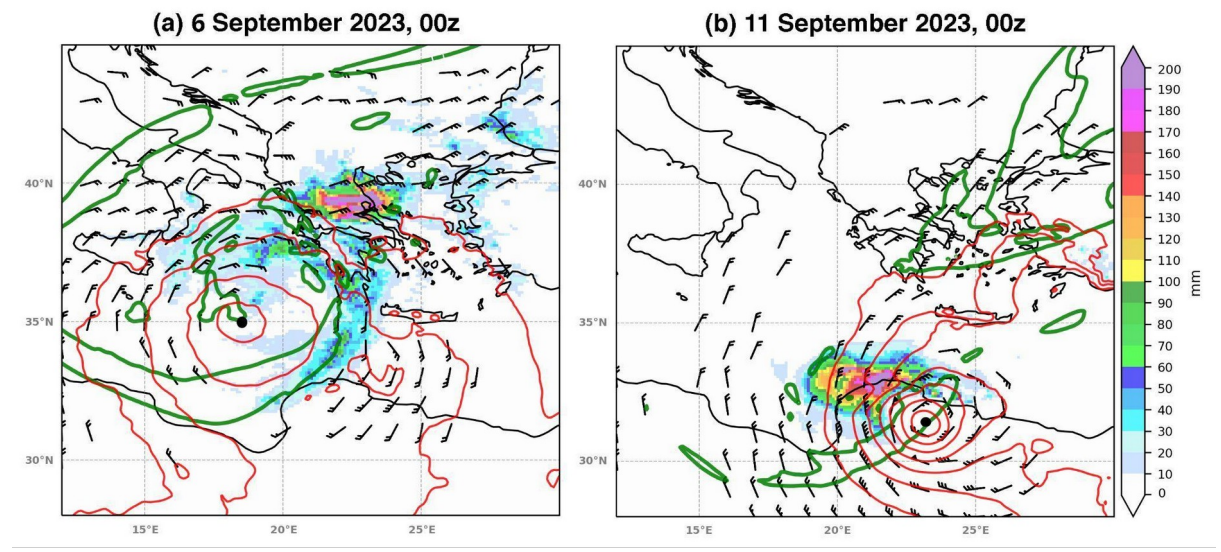


**Figure 2 (a)** Potential Vorticity of 2 PVU at 300 hPa (in green contour) and wind speed higher than 15 knots at 850 hPa (in barbs, with full and half bars depicting 10 and 5 knots, respectively) and MSLP (in red contours for values lower than 1012 hPa with 2 hPa interval) on 6 September 2023, at 00 UTC. 24-hour total accumulated precipitation from 5 to 6 of September 00 UTC is shown in shading (max value 434 mm). **(b)** Same as **(a)** but for 11 September 2023, at 00 UTC (max precipitation value 382 mm). The black dot indicates the minimum MSLP position in both panels.

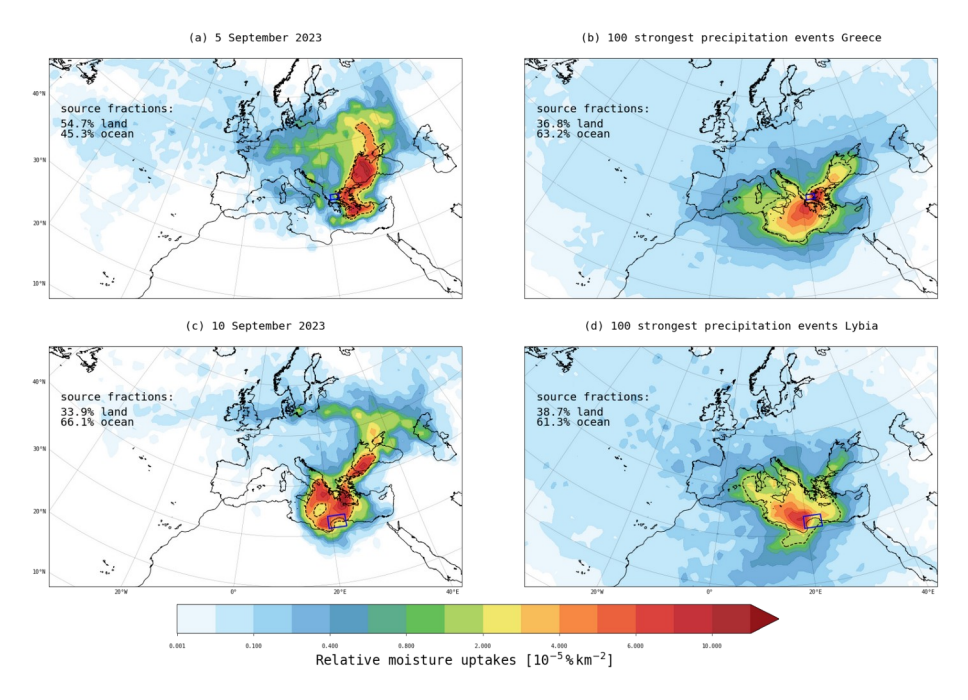


**Figure 3 (a) Relative** moisture uptakes that contribute to the precipitation event in Thessaly (depicted with the blue rectangle) on 5 September 2023. The black dashed contour outlines the largest moisture source regions, which account for 50% of the total moisture uptake. The numbers on the top left show the relative land and ocean fraction of the moisture sources. **(b)** as in **(a)** but for the 100 most extreme daily precipitation events in Thessaly from 1990 to 2023. **(c)** as in **(a)** but for the precipitation in the study region in Libya (blue rectangle) on 10 September 2023. **(d)** as in **(b)** but for Libya.

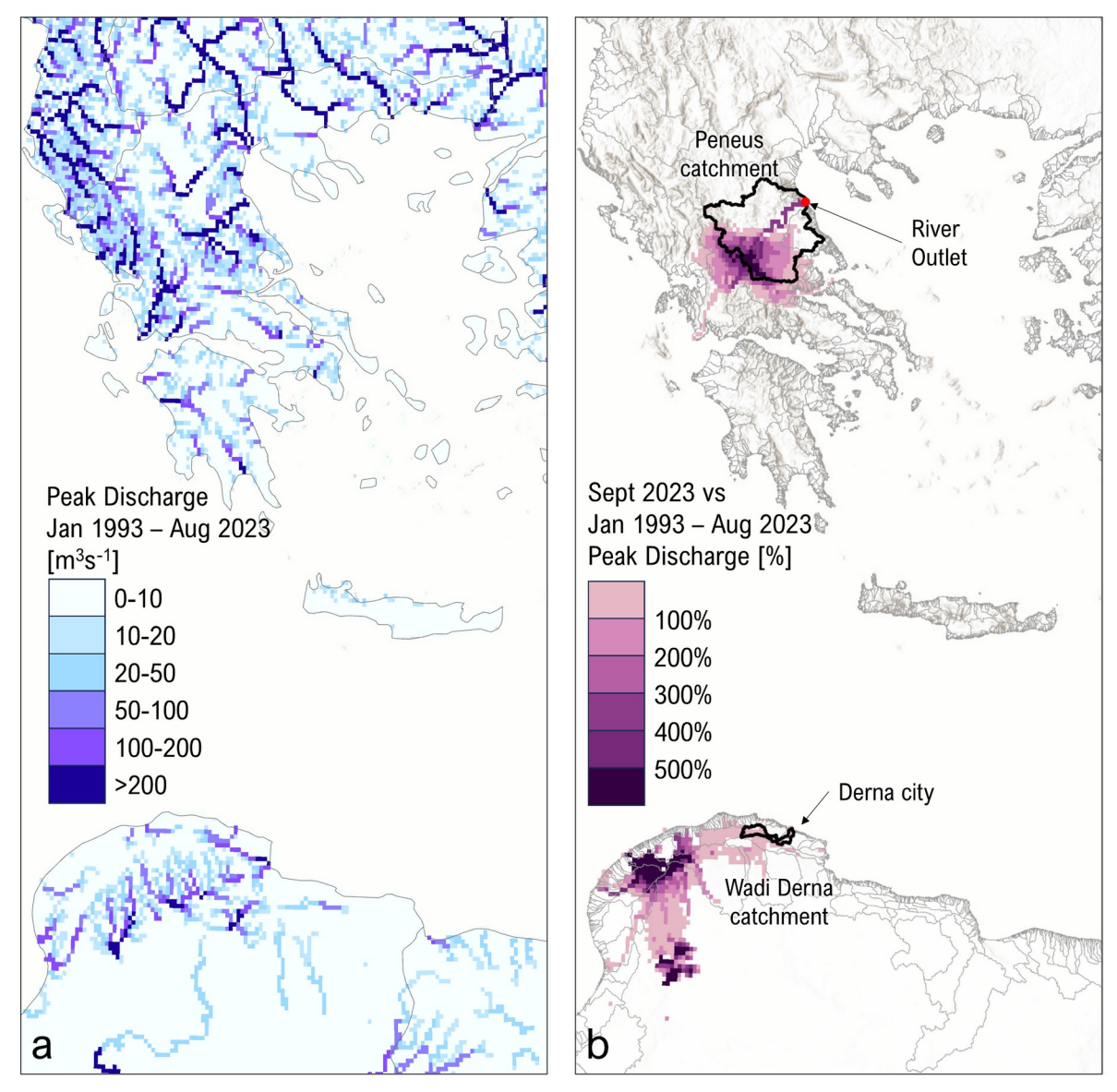


**Figure 4** Peak discharge over three recent decades (Jan 1993 – Aug 2023) versus Daniel storm as represented by the Global Flood Awareness System (a) spatial distribution of the maximum peak river discharge from January 1993 to August 2023, (b) comparison map for September 2023 illustrating the event-wide peak river discharges as a percentage increase over the maximum peak river discharges during the 30 years January in (a).

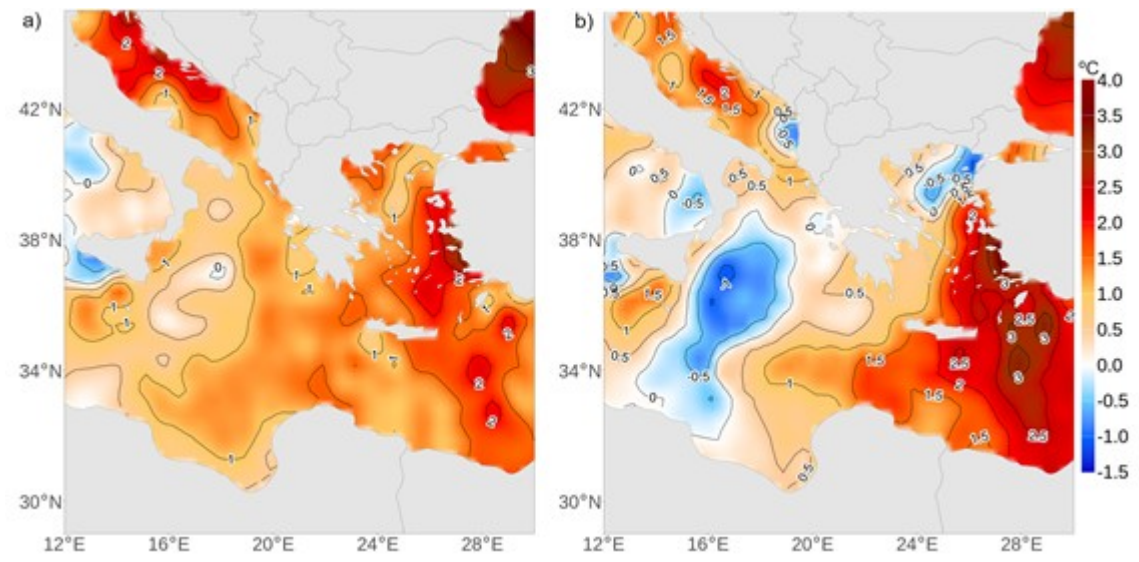


**Figure 5 (a)** Daily SST anomaly from ERA5, for 3 September 2023, and (b) 9 September 2023. The reference climatology for anomaly determination is 1982-2011.

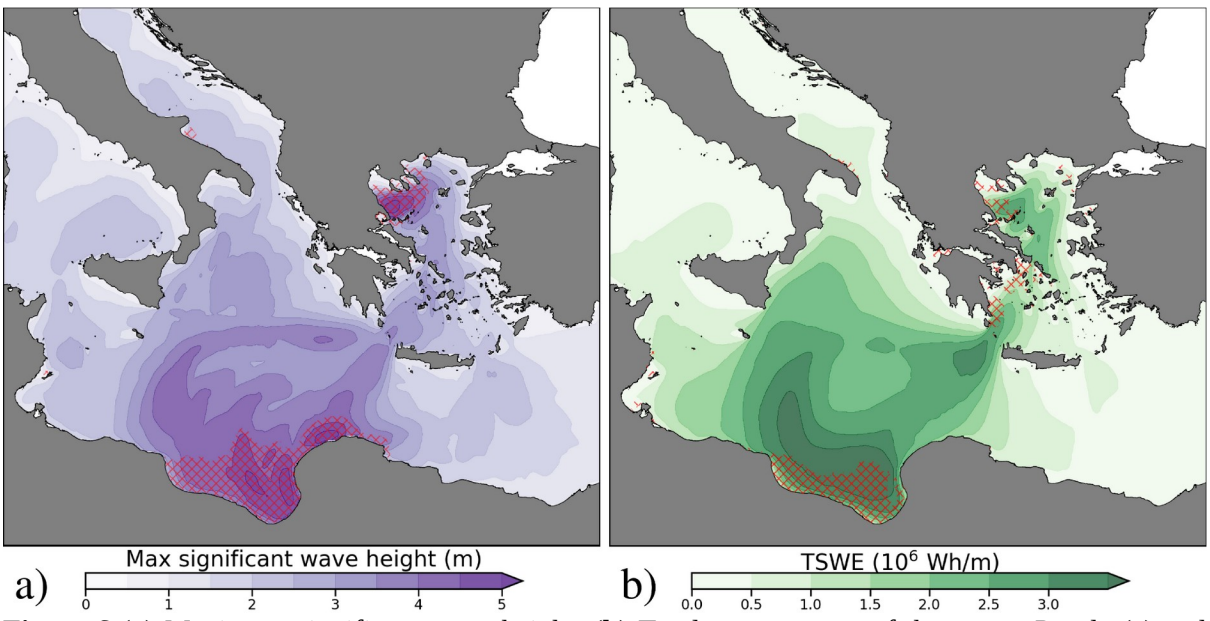


**Figure 6 (a)** Maximum significant wave height. **(b)** Total wave energy of the storm. Purple (a) and red (b) patches mark areas of extreme conditions (above the 99th percentile) determined based on the Mediterranean Sea wave reanalysis.

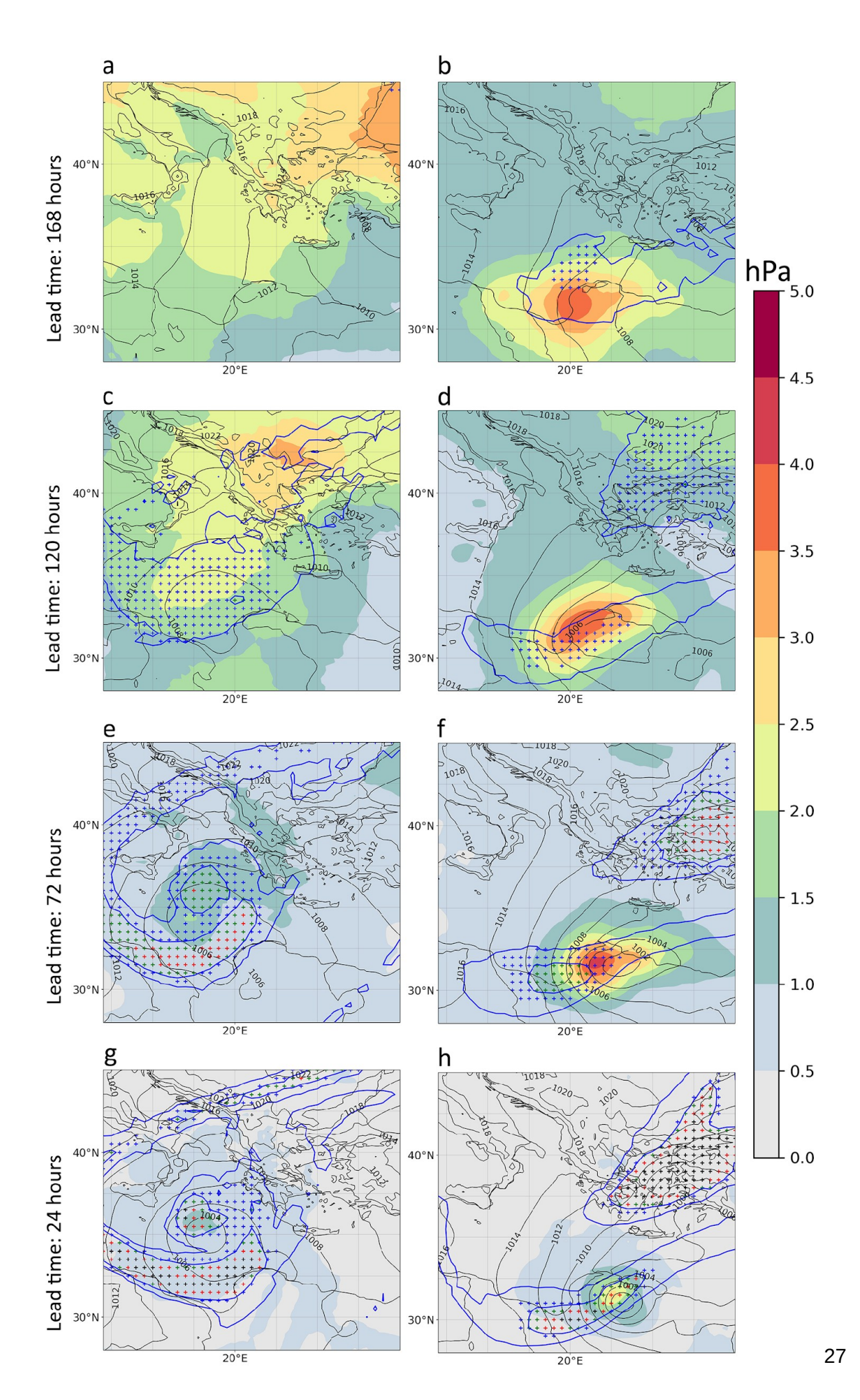


**Figure 7** Standard deviation (in colour shading) and average (in black contour) MSLP from the 51 ensemble members of the ECMWF EPS. Blue contours enclose areas with a median equal to 1 and 2 PVU at 300 hPa among all members of the EPS. Blue crosses indicate areas where at least 25% of the members have PV values greater than 2 PVU. Green, red, and black crosses denote agreement by at least 50%, 75%, and 95% of the members, respectively. Panels depict different lead forecast times valid on 6 September at 00 UTC (panels **a**, **c**, **e**, **g**) and 11 September at 00 UTC (**b**, **d**, **f**, **h**).

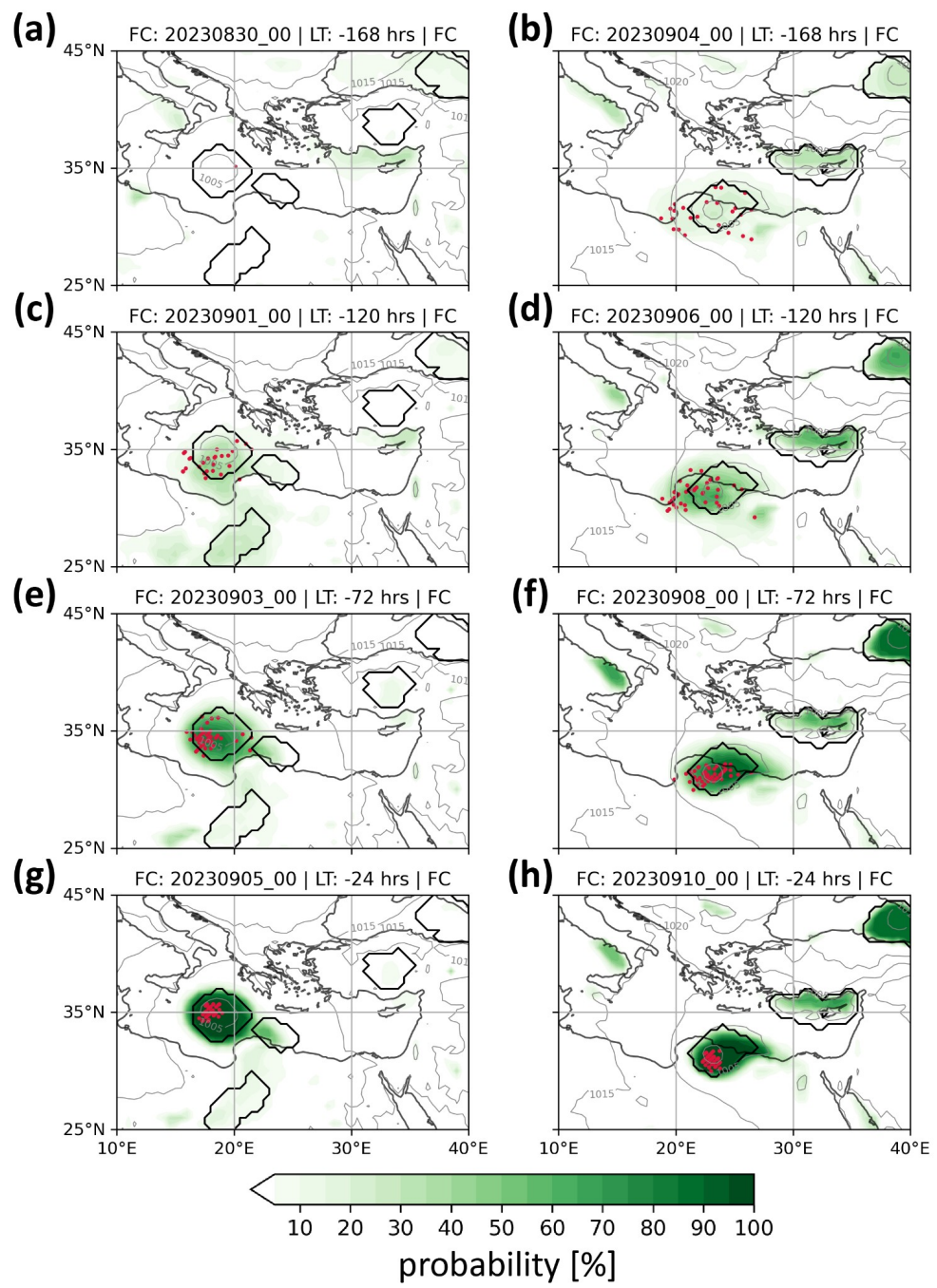


**Figure 8** Percentage of overlapping cyclone objects (green shading) among the ensemble prediction system members for different lead times valid on 6 September 2023, 00 UTC (left column panels) and 11 September 2023, 00 UTC (right column panels). Black contours show cyclone objects in ECMWF analysis (grey contours for MSLP isobars in ECMWF analysis). Red dots depict the location of the minimum MSLP of Daniel in the ensemble members.

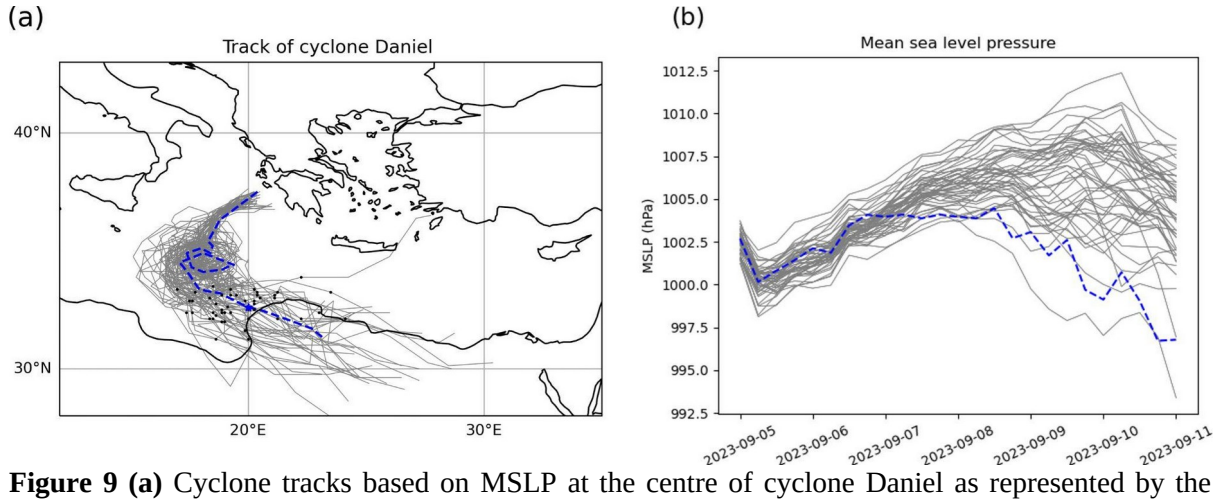


**Figure 9 (a)** Cyclone tracks based on MSLP at the centre of cyclone Daniel as represented by the ECMWF analysis (blue dashed line) and by the 50 members of the EPS of ECMWF (grey lines), initialized on 5 September at 00 UTC. Black dots in (a) depict the cyclone location on 10 September, 00 UTC (b) As in (a) but as time series of minimum MSLP.

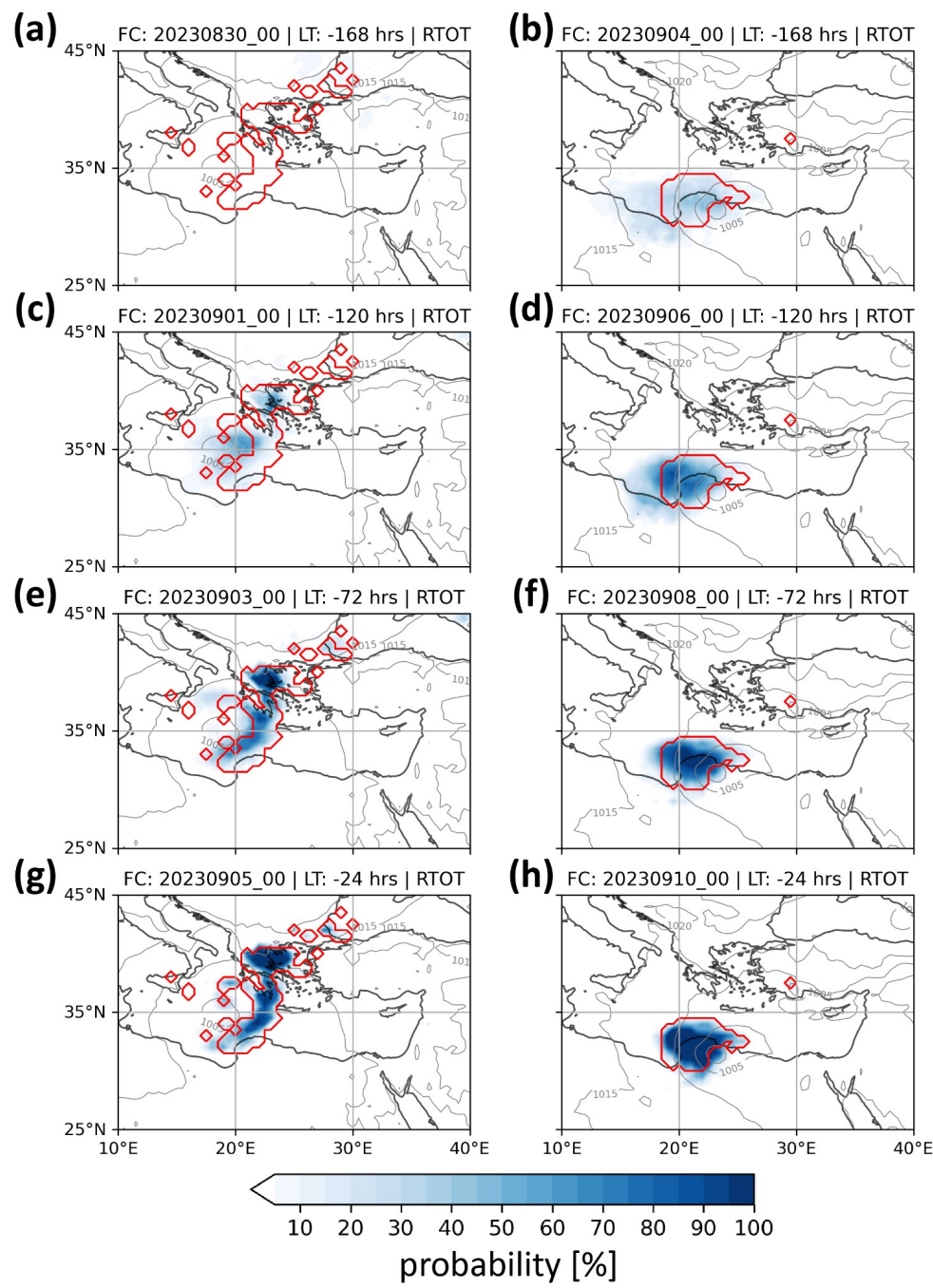


**Figure 10** Percentage of overlapping objects (in blue shading) among the ensemble prediction members for 24-hour accumulation (ending at the validity time) of extreme precipitation for different lead times valid on 6 September 2023, 00 UTC (left column panels) and 11 September 2023, 00 UTC (right column panels). Red contours show objects of extreme precipitation determined based on ERA5 climatology (grey contours for MSLP isobars in ECMWF analysis).

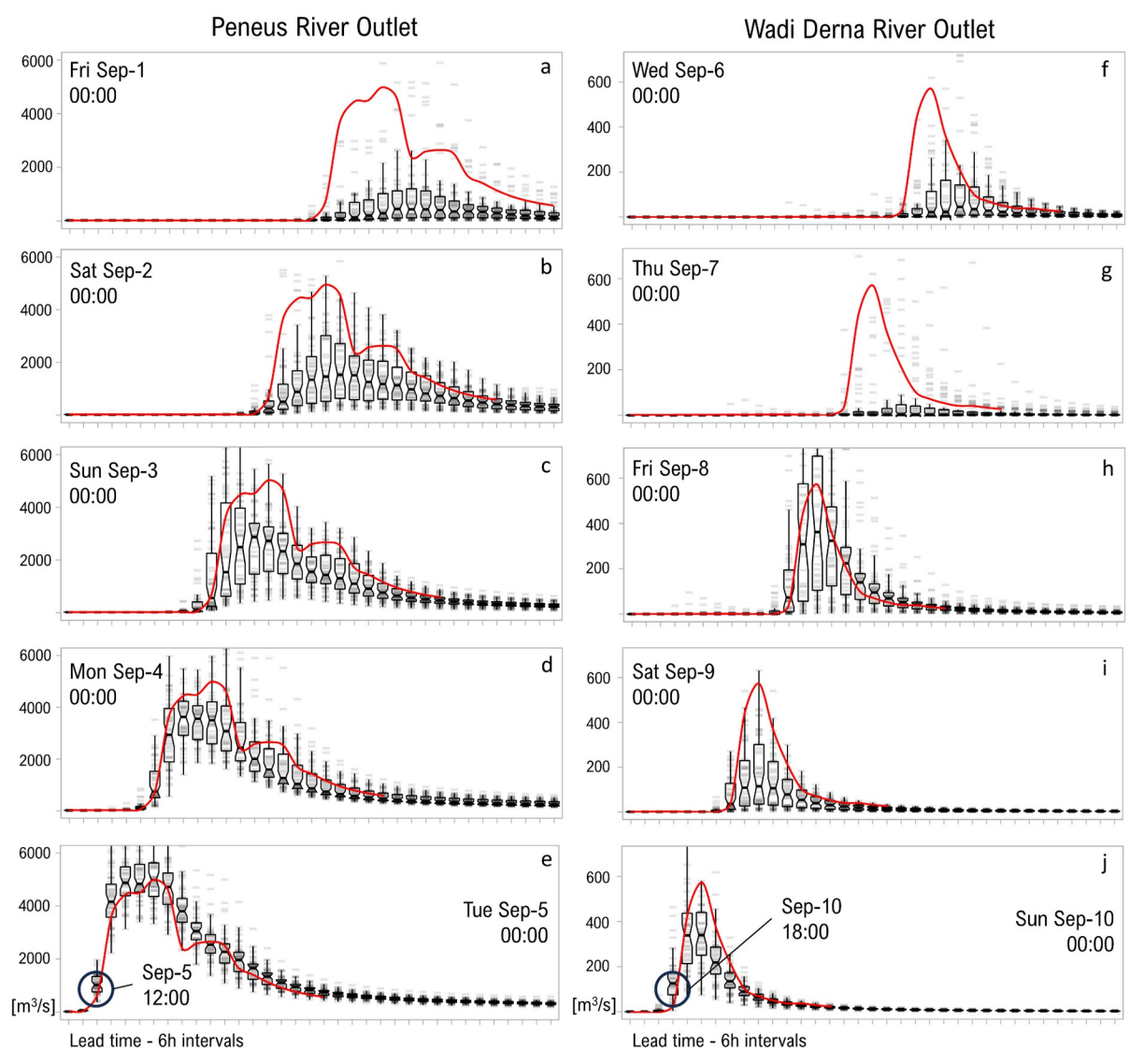


**Figure 11** Six-hourly ensemble river discharge forecasts for the Peneus and Wadi Derna catchments compared to the "perfect forecast" benchmark (red line). The "perfect forecast" represents the initialization of each forecast for all time steps across the event, taken as a reference for evaluating forecast accuracy. With the observed timing of rising hydrograph limbs marked on 5 September, noon local time (09 UTC) for the Peneus River in Thessaly, and 10 September, 18:00 local time (16 UTC) for the Wadi Derna River. Grey stripes (tick marks) represent individual ensemble members from the EFAS model, driven by the 51 ensemble members of the ECMWF EPS. Overlapping tick marks darken, visually highlighting areas of member agreement (convergence). Forecast summary data are displayed as boxplots, where the box represents the interquartile range (IQR), the whiskers show the range of values within 1.5 times the IQR, and the horizontal black line inside the box indicates the median. The notches around the median show the 95% confidence interval.

1303

1304

1305

1306

1307

1308

1309

1310

1311

1312

1313

1314

1315

1316

1317

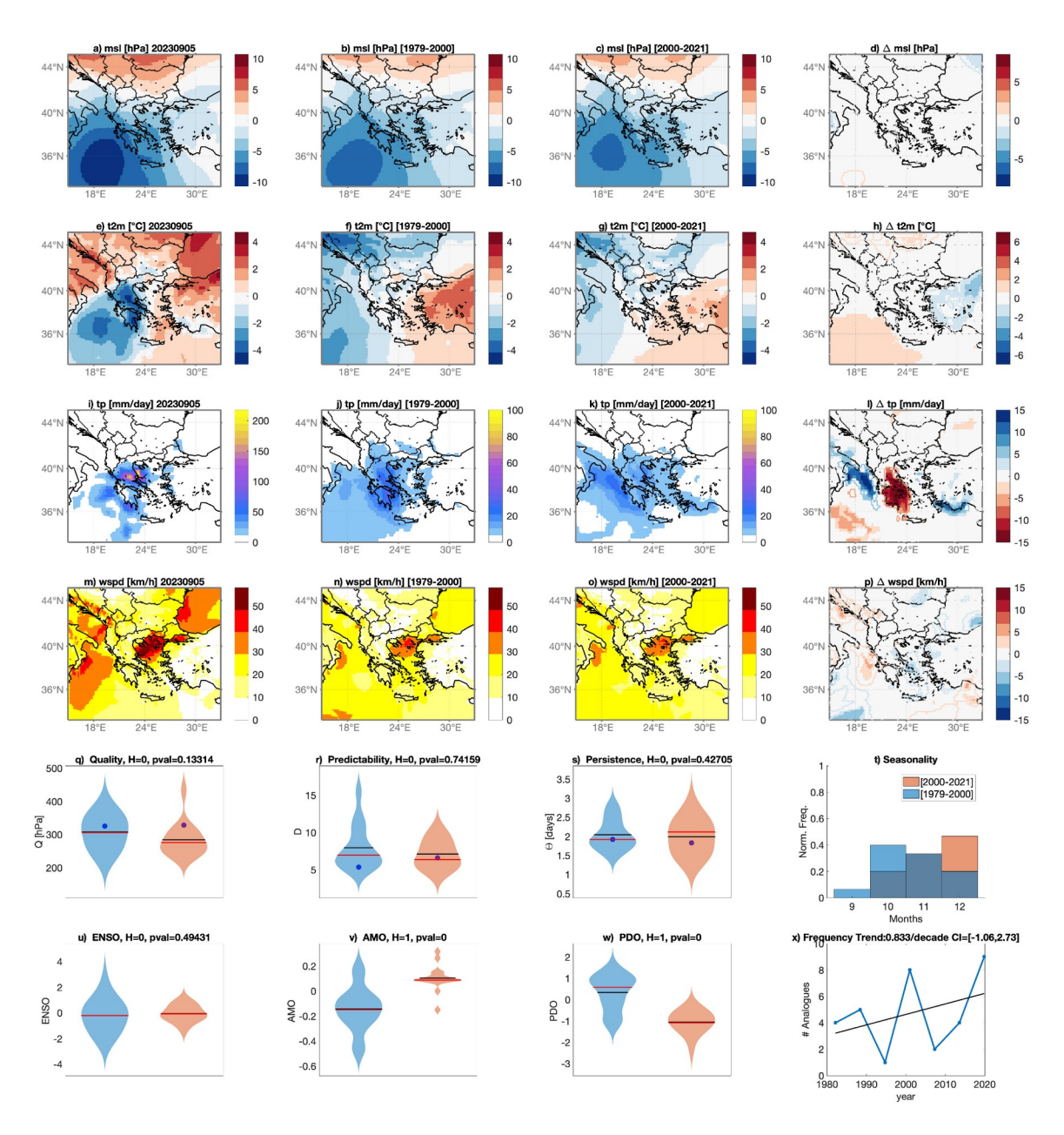


Figure 12: Analogues for 5 September 2023 and the region [15°E-33°E, 33°N-45°N] and the extended autumn season SOND: average surface pressure anomaly (msl) (a), average 2-m temperature anomalies (t2m) (e), accumulated total precipitation (tp) (i), and average wind-speed (wspd) in the period of the event. Average of the surface pressure analogs found in the counterfactual [1979-2000] (b) and factual periods [2001-2022] (c), along with corresponding 2-m temperatures (f, g), accumulated precipitation (j, k), and wind speed (n, o). Changes between present and past analogs are presented for surface pressure  $\Delta msl$  (d), 2-m temperatures  $\Delta t2m$  (h), total precipitation  $\Delta tp$  (i), and wind speed  $\Delta$ wspd (p): color-filled shaded areas indicate significant anomalies obtained from the bootstrap procedure. Contours indicate non-significant changes; Violin plots for past (blue) and present (orange) periods for Quality Q analogs (q), Predictability Index D (r), Persistence Index  $\Theta$  (s), and distribution of analogs in each month (t). Violin plots for past (blue) and present (orange) periods for ENSO (u), AMO (v) and PDO (w). Number of the Analogues occurring in each subperiod (blue) and linear trend (black). A blue dot marks values for the peak day of the extreme event. Horizontal bars in panels (q,r,s,u,v,w) correspond to the mean (black) and median (red) of the distributions. (x) number of analogues found in sub periods of ~6 years when 33 analogues are searched in the whole period 1979-2022.

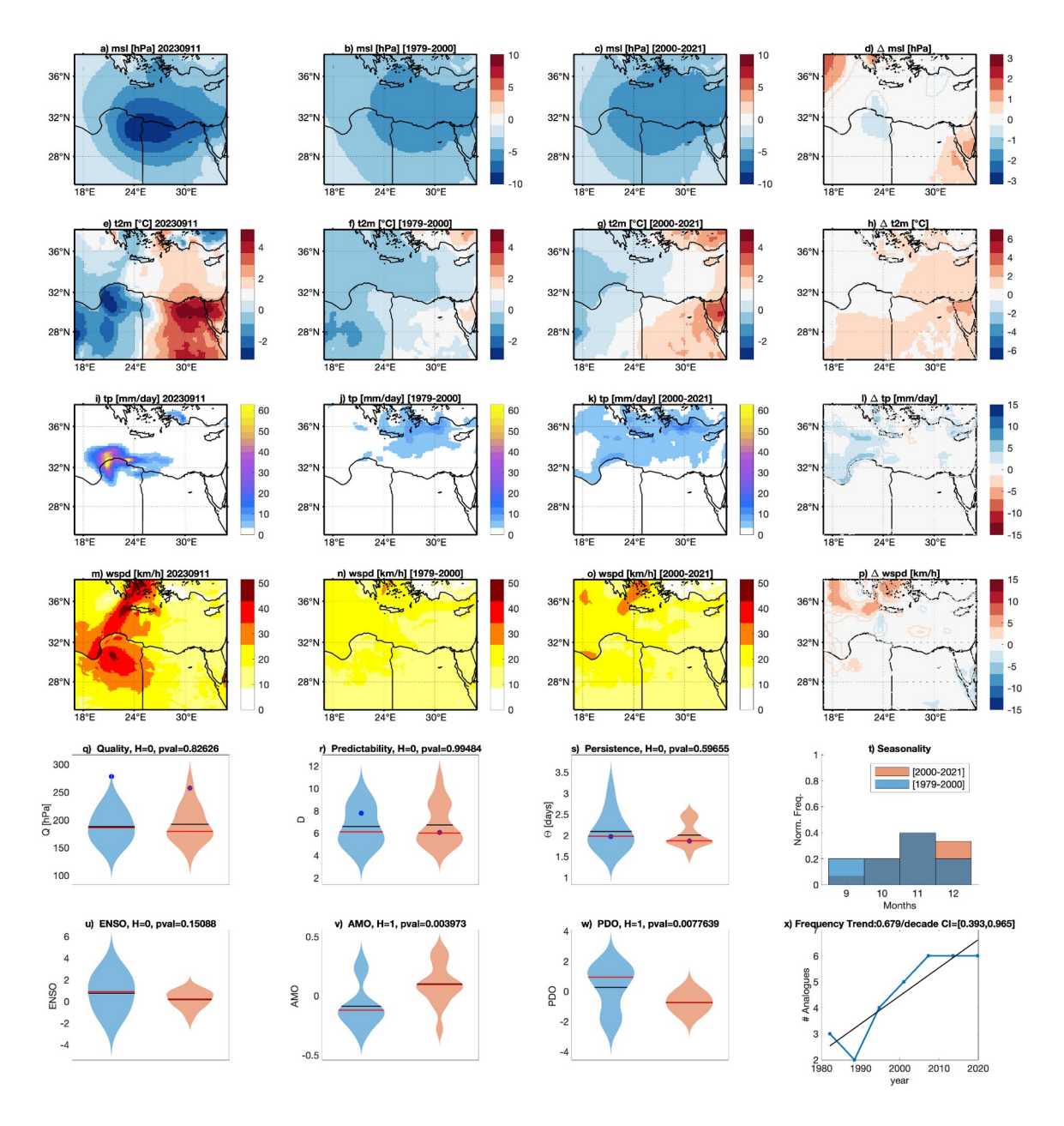


Figure 13: As in Fig. 12, but for 10-11 September 2023, the region [17°E-35°E, 25°N-38°N] and the extended autumn season (SOND).

1322